Department of Applied Physics

Influence of vacancy defects on the optical properties of natural diamond and aluminium nitride

Jussi-Matti Mäki

Aalto University

DOCTORAL DISSERTATIONS

Aalto University publication series
DOCTORAL DISSERTATIONS 28/2012

Influence of vacancy defects on the optical properties of natural diamond and aluminium nitride

Jussi-Matti Mäki

Doctoral dissertation for the degree of Doctor of Science in Technology to be presented with due permission of the School of Science for public examination and debate in Auditorium K at the Aalto University School of Science (Espoo, Finland) on the 30th of March 2012 at 13 o'clock.

Aalto University
School of Science
Department of Applied Physics

Supervisor
Prof. Martti Puska

Instructor
Dr. Filip Tuomisto

Preliminary examiners
Prof. Seppo Honkanen, University of Eastern Finland
Prof. Reinhard Krause-Rehberg, University Halle, Germany

Opponent
Dr. Tim Veal, University of Liverpool, UK

Aalto University publication series
DOCTORAL DISSERTATIONS 28/2012

© Jussi-Matti Mäki

ISBN 978-952-60-4545-0 (printed)
ISBN 978-952-60-4546-7 (pdf)
ISSN-L 1799-4934
ISSN 1799-4934 (printed)
ISSN 1799-4942 (pdf)

Unigrafia Oy
Helsinki 2012

Finland

The dissertation can be read at http://lib.tkk.fi/Diss/

441 697
Printed matter

Aalto University

Abstract

Aalto University, P.O. Box 11000, FI-00076 Aalto www.aalto.fi

Author
Jussi-Matti Mäki

Name of the doctoral dissertation
Influence of vacancy defects on the optical properties of natural diamond and aluminium nitride

Publisher School of Science

Unit Department of Applied Physics

Series Aalto University publication series DOCTORAL DISSERTATIONS 28/2012

Field of research Experimental physics

Manuscript submitted 8 December 2011 **Manuscript revised** 22 February 2012

Date of the defence 30 March 2012 **Language** English

☐ **Monograph** ☒ **Article dissertation (summary + original articles)**

Abstract

Vacancy defects affect the optical properties of semiconductors in many ways. The defects form deep energy levels in the band gap acting either as a charge carrier recombination or generation centres. This is seen as absorption of light. In this thesis, the vacancy defects in diamond and aluminium nitride (AlN) and their influence on the optical properties have been studied using positron annihilation spectroscopy. A new method, optical transient positron spectroscopy, was developed for this purpose.

A large fraction of the purest natural diamonds have a smoky brown tint. The brown colour can be removed in high pressure, high temperature (HPHT) treatments. The positron measurements presented in this thesis show that brown natural diamond contains a large concentration of clusters of 40-60 missing atoms. Optical wavelength photons excite electrons to the vacancy clusters, which causes the visible absorption and the smoky-brown colour of the diamond. Further, it was detected that vacancy cluster concentration decreases in correlation with the removal of the brown colour during the HPHT treatments. The decay of the excitation after switching off the illumination is very slow, taking several minutes. By combining flux-dependent measurements with the decay rates of the photoexcitation effects, the optical cross section of the clusters causing the brown colouration can be determined and the vacancy cluster concentration estimated self-consistently.

Vacancy defects were studied in single-crystal bulk AlN substrates. Al vacancy-related positron signals (lifetime, Doppler broadending) are identified and the vacancy charge state was confirmed to be negative. By combining coincidence-Doppler broadening measurements with ab-initio theoretical calculations it is shown that in-grown Al vacancies are present as complexes with oxygen impurities, while high-energy particle irradiation produces predominantly isolate Al vacancies. Optical absorption measurements show that the latter cause absorption at ultraviolet wavelengths, important from the point of view of employing AlN as substrate material for opto-electronic devices.

Keywords Positrons, defects, optical properties, diamond, aluminium nitride

ISBN (printed) 978-952-60-4545-0 **ISBN (pdf)** 978-952-60-4546-7

ISSN-L 1799-4934 **ISSN (printed)** 1799-4934 **ISSN (pdf)** 1799-4942

Location of publisher Espoo **Location of printing** Helsinki **Year** 2012

Pages 122 **The dissertation can be read at** http://lib.tkk.fi/Diss/

A! Aalto-yliopisto

Tiivistelmä

Aalto-yliopisto, PL 11000, 00076 Aalto www.aalto.fi

Tekijä
Jussi-Matti Mäki

Väitöskirjan nimi
Vakanssivirheet ja niiden vaikutus optisiin ominaisuuksiin luonnontimantissa ja alumiininitridissä

Julkaisija Perustieteiden korkeakoulu

Yksikkö Teknillisen fysiikan laitos

Sarja Aalto University publication series DOCTORAL DISSERTATIONS 28/2012

Tutkimusala Kokeellinen fysiikka

Käsikirjoituksen pvm 08.12.2011 **Korjatun käsikirjoituksen pvm** 22.02.2012

Väitöspäivä 30.03.2012 **Kieli** Englanti

☐ **Monografia** ☒ **Yhdistelmäväitöskirja (yhteenveto-osa + erillisartikkelit)**

Tiivistelmä

Vakanssivirheet vaikuttavat puolijohteiden ominaisuuksiin monin tavoin. Yksi vakanssien huomattavammista vaikutuksista on niiden aiheuttamat muutokset puolijohteen optisiin ominaisuuksiin. Vakanssivirheet muodostavat puolijohteen kiellettyyn energiaväliin tiloja, jotka voivat toimia absorptio- tai rekombinaatiokeskuksina. Paljaalle silmälle tämä näkyy esim. värin muutoksena verrattuna virheettömään kiteeseen. Tässä väitöskirjassa on tutkittu vakanssivirheitä timantissa ja alumiininitridissä (AlN) ja etenkin virheiden vaikutusta aineen optisiin ominaisuuksiin.

Suurimmalla osalla puhtaimmista luonnontimanteista on ruskeahko värinsävy. Väristä päästään eroon käsittelemällä timantteja suuressa paineessa ja lämpötilassa (ns. HPHT-käsittely). Tässä väitöskirjassa esitetyt positronimittaukset ovat paljastaneet, että ruskeat timantit sisältävät suuren konsentraation n. 40-60 puuttuvan atomin vakanssiklustereita. Valaisemalla näytteitä havaittiin positronin elinajan kasvavan. Tämä viittaa siihen, että elektroneja virittyy klustereihin, aiheuttaen timanttien ruskeahkon värin. Lisäksi havaittiin, että HPHT-käsittelyn jälkeen vakanssiklusterikosentraatio pienenee korrelaatiossa ruskean värin poistumisen kanssa. Valaisun jälkeen positronin elinaika pysyy koholla hyvin pitkään, useita minuutteja. Ilmiön tarkempaab tutkimiseen kehitettiin laitteisto vakanssiin virittyneiden elektronien rekombinaationopeuden mittaamisen. Yhdistämällä tieto valaisuefektin vuoriippuvuudesta ja elektronien rekombinaationopeudesta, saatiin määriteltyä ruskean värin aiheuttavien vakanssiklustereiden absorptiovuorovaikutusala ja tätä kautta lopulta defektien konsentraatio näytteissä.

Väitöstutkimuksessa mitattiin erilliskiteistä AlN:iä. Mittauksissa identifioitiin alumiinivakanssi, sekä saatiin viitteitä alumiinivakanssin negatiivisesta varaustilasta. Mittaamalla AlN-näytteitä koinsidenssi-Dopplerilla ja vertailemalla tuloksia teoreettisiin laskuihin havaittiin, että AlN-erilliskiteissä Al-vakanssit ovat kompleksoituneet happiatomien kanssa. Optiset mittaukset paljastivat, että erilliset Al-vakanssit aiheuttavat absorptiota ultraviolettiaallonpituuksilla.

Avainsanat Positronit, hilavirheet, optiset ominaisuudet, timantti, alumiininitridi

ISBN (painettu) 978-952-60-4545-0 **ISBN (pdf)** 978-952-60-4546-7

ISSN-L 1799-4934 **ISSN (painettu)** 1799-4934 **ISSN (pdf)** 1799-4942

Julkaisupaikka Espoo **Painopaikka** Helsinki **Vuosi** 2012

Sivumäärä 122 **Luettavissa verkossa osoitteessa** http://lib.tkk.fi/Diss/

Preface

The work presented in this thesis was conducted in the positron group of Department of Applied Physics of Aalto University between the years 2006 and 2011.

I wish to express my gratitude to my instructor Doc. Filip Tuomisto for his help and guidance during the long process of doing the research presented in this thesis. I thank the late professor Kimmo Saarinen for taking me into the positron group as summer student back in 2004. I wish to thank Professors Martti Puska and Pekka Hautojärvi for supervising the research. I am grateful to Dr. Klaus Rytsölä for his help in solving the plentiful experimental problems I have encountered. Further, I am indebted to several people who have helped me during various stages of the research, too long a list to mention here. Financial support from the Vilho, Yrjö and Kalle Väisälä Foundation is gratefully acknowledged.

Special thanks goes to the current and past people of the positron research group for the pleasant working atmosphere. Special thanks to Floris Reurings for helping with the English grammar and to the skipper Jonatan Slotte for the annual sailing trips.

I wish to thank all the people around me while out of office. Thanks goes to my parents and to all my friends. Finally and most importantly, thank you Henna for all the support and encouragement.

Helsinki, February 29, 2012,

Jussi-Matti Mäki

Contents

This thesis consists of an overview and the following publications:

I J.-M. Mäki, F. Tuomisto, C.J. Kelly, D. Fisher, and P.M. Martineau, *Properties of optically active vacancy clusters in type IIa diamond*, Journal of Physics: Condensed Matter **21**, 364216, pages 1-10 (2009).

II J.-M. Mäki, F. Tuomisto, A. Varpula, D. Fisher, R.U.A Khan, and P.M. Martineau, *Time dependence of charge transfer processes in diamond studied with positrons*, Physical Review Letters, 107, 217403, pages 1-5 (2011).

III J.-M. Mäki, T. Kuittinen, E. Korhonen, and F. Tuomisto, *Positron lifetime spectroscopy with optical excitation: case study of natural diamond*, New Journal of Physics, accepted for publication, pages 1-15 (2012).

IV F. Tuomisto, J.-M. Mäki, T.Yu. Chemekova, Yu.N. Makarov, O.V. Avdeev, E.N. Mokhov, A.S. Segal, M.G. Ramm, S. Davis, G. Huminic, H. Helava, M. Bickermann, B.M. Epelbaum, *Characterization of bulk AlN crystals with positron annihilation spectroscopy*, Journal of Crystal Growth **310**, 3998-4001 (2008).

V J.-M. Mäki, I. Makkonen, F. Tuomisto, A. Karjalainen, S. Suihkonen, J. Räisänen, T. Yu. Chemekova, and Yu. N. Makarov, *Identification of the VAl-ON defect complex in AlN single crystals* Physical Review B (R), **84**, 081204, pages 1-4 (2011).

The author, Jussi-Matti Mäki, has actively contributed to the experimental positron annihilation studies presented in this thesis. He has conducted the positron measurements and the analysis of the experimental data in all the publications in the thesis, and the theoretical calculations in Publ **I**. He is the corresponding author of Publs. **I-III** and Publ. **V**. Furthermore, he was the main contributor in the design, construction, and testing of the new optical positron measurement setup applied in Publs. **II-III**.

1. Introduction

The semiconducting materials studied in this thesis, AlN and diamond, are two of the most extreme in many of their properties. Both are composed of small, strongly bonded atoms, which results in a wide band gap and very stable structural properties [1]. However, the high cohesion energy of both means that the synthesis is very difficult and resulting materials contain many crystallographic defects. This is naturally a fertile ground for the characterization of the defects!

Diamond is a group IV elemental semiconductor [2]. It has an indirect band gap, like its relatives in the group IV: Si and Ge. In contrast, AlN is a direct band gap semiconductor as the other III-nitrides, making it an attractive choice for optoelectronic applications [3]. The band gap of diamond, 5.5 eV, is much wider than that of Si and Ge, as shown in figure 2.1. The band gap of AlN is even wider at 6.2 eV, much more than those of InN and GaN.

Even though there are many similarities between diamond and AlN, the fundamental difference between a direct and an indirect band gap makes their potential applications quite different. Diamond is a promising material for high power and high frequency power electronics due to its high carrier mobility and excellent thermal and mechanical stability. However, the high price of diamond single crystals and the lack of a natural oxide means that it is not going to replace silicon in mainstream consumer applications. Additionally, efficient n-type doping is a challenge yet to be overcome [4]. Potential applications of AlN-based optoelectronics include far-UV semiconductor lasers and light emitting diodes (LEDs) either as pure AlN or as a compound with other nitrides. Emission of 210 nm radiation using AlN LEDs has already been reported, albeit with a very low efficiency [5]. Additionally, AlN is a very promising substrate material for other nitrides, where its good thermal conductivity can be taken advantage of.

In this thesis, vacancies in AlN and diamond are studied, especially from

the viewpoint of their optical properties. Diamond has for long attracted people by its mechanical hardness, rarity in nature, and especially its sparkle. The sparkle originates from diamond's high index of refraction, $n = 2.42$ [6]. However, a big portion of natural diamond crystals exhibit a smoky-brown tint, making them less attractive and thus less valuable as gemstones. The identification of the origin of the brown colour has been lacking, despite being extensively studied. Natural diamond is also an interesting material from the point of view of positron annihilation spectroscopy, as the decay of the optical charge transfer process is slow and the lifetime component related to the optical effect can easily be extracted from the positron lifetime spectrum. A new positron measurement technique has been developed in order to study the optical effect in detail. In the case of AlN, the in-grown and irradiation induced vacancy defects are identified. Further, the influence of different vacancy types to the ultraviolet (UV) transparency of AlN substrates is studied.

Positron measurements provide information about the vacancy structure, concentration, and charge state [7, 8, 9, 10]. Both positron lifetime spectroscopy and Doppler broadening spectroscopy have been employed in this thesis. Furthermore, the combination of experimental measurements and ab-initio theoretical calculations has been used to obtain information on the chemical surrounding of the vacancy [11]. The optical properties of vacancies can be studied by illuminating the sample *in situ* during the positron measurements.

In Publ. I the origin of the brown colour in natural type IIa (high purity diamond with less than 10^{16} cm^{-3} nitrogen present) is studied. We show that the brown colour is related to vacancy clusters of roughly 40-60 missing atoms causing a positron lifetime component of 400 ps. The vacancy clusters disappear during high pressure high temperature (HPHT) treatment, as is evident from the disappearance of the 400 ps component in stages during the anneal. This is in correlation with the reduction of brown colour (optical absorption), suggesting that the clusters dissociate when the brown colour is lost.

The optical properties of the vacancy clusters in natural diamond are further studied in Publs. II and III with optical transient positron spectroscopy. We have developed a setup where a light pulse is injected into the sample and the decay of the optical effect is measured with positron lifetime spectroscopy. Combining the transient measurements with steady state illumination measurements we obtain an estimate of the optical cross section of the vacancy clusters. Further, the decay of the optical effect provides information on the recombination dynamics of the system. The results obtained with the transient positron measurements are compared to transient photoconductivity, yielding

similar recombination rates.

Finally, in Publs. IV and V, Al vacancies in physical vapour transport (PVT) grown AlN single crystals are studied. Negative Al vacancies are identified in Publ. IV with positron lifetime spectroscopy. Additionally, a high concentration of negative ions is detected. In Publ. V it is determined that the in-grown negative Al vacancies are decorated by oxygen atoms. The identification is done by combining coincidence Doppler broadening spectroscopy with ab-initio calculations. Further, isolated Al vacancies are identified in proton irradiated AlN.

2. Wide band-gap semiconductors, defects and optical properties

The forbidden energy (or the band gap) of a semiconductor is the energy separating the valence and conduction bands, i.e., a gap where there are no electronic states. The band gap is the energy required to free an electron from the bond to become a mobile charge carrier. An electron can be excited, e.g., thermally or optically to become mobile. The importance of semiconductors in technological applications is based on the fact that the charge carrier density can be controlled by adding impurity atoms to the material and creating additional electronic states in the band gap, called doping.

The value of the band gap tends to correlate with the lattice constant, because small atoms typically have a stronger Coulombic attraction between electrons and the ion core. This is the case with diamond with its 5.5 eV gap. In AlN the band gap is even larger, 6.2 eV, due to nearly ionic bonds. The band gap versus the lattice parameter in different III-nitride and group-IV semiconductors is plotted in figure 2.1. The strong atomic bonds result in the high mechanical and thermal stability of both diamond and AlN. For example the thermal conductivity [12] and radiation hardness [13] are very high.

Defects break the periodicity of a semiconductor material, introducing discrete energy levels in the band gap. Such defects include impurity atoms, dislocations, interstitials, vacancies, stacking faults, and precipitates. The defects affect the electrical and optical properties of (opto)electronic devices by trapping charge carriers, absorbing photons, and degrading the luminescence properties, etc. Additionally the mechanical and thermal properties of semiconductors suffer from the presence of the defects. The knowledge of identities and concentrations of vacancy defects are important in understanding the material properties.

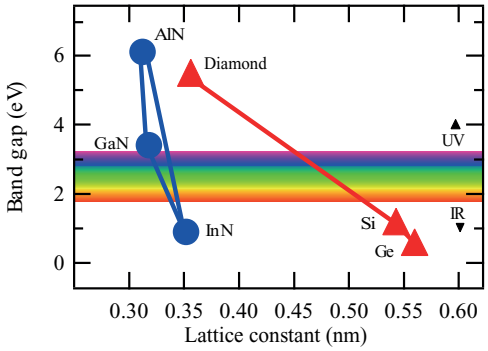

Figure 2.1. Lattice constant versus the forbidden energy gap in III-nitrides and IV-semiconductors [1]. The optical (visible) part of the electromagnetic spectrum ranges roughly from 1.8 to 3.1 eV.

2.1 Diamond

Diamond is composed of tetrahedrally bonded carbon atoms. The diamond lattice structure is illustrated in figure 2.2. Diamond has a density of 3.52 g/cm^3, a lattice constant of $a = 3.57$ Å and an indirect band gap of 5.5 eV [6, 1]. Carbon is present in nature and can be synthesised in several allotropes. This is due to the fact that the four valence electrons of carbon can form several bond types. Of all the allotropes, diamond is the most valued one. Many properties of diamond are very extreme, for example the hardness and the index of refraction. Diamond is additionally very rare in nature. In the diamond lattice one of the atomic s-orbitals and three p-orbitals are hybridised to sp^3-orbitals, resulting in four very stable covalent bonds that are oriented at angle of 109,5° with respect to each other. The most abundant allotrope of carbon, however, is graphite, which consists of sp^2 hybridised sheets of carbon. It is interesting to compare the properties of graphite to those of diamond. Graphite sheets are only weakly bound to each other by the van der Waals interaction, which means that graphite is one of the softest solid state materials. It is also a good conductor due to the fact that one of the p orbitals is free to form π bonds with neighbouring C atoms and thus to conduct electricity.

The use of diamond in industry has been limited to mechanical applications, for example drilling or cutting, while the lack of high quality synthetic material with controlled n- and p-type doping has hindered the use in electronics. Only very recently has the quality of synthetic diamonds begun to approach the standards required for electronic applications [14, 15]. However, there are still several hurdles before the realization of industrial-scale diamond-based electronics.

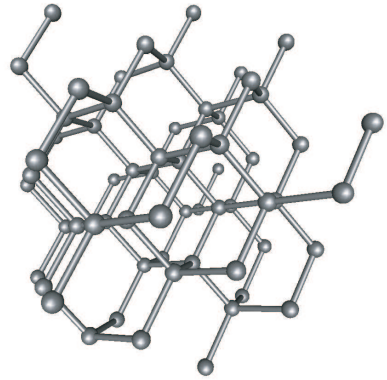

Figure 2.2. Illustration of the diamond lattice.

2.1.1 Defects in diamond

There are several types of defects present in diamond. In the case of natural diamond, this is partially due to the fact that natural diamond originates from the mantle of the earth, thus very often being plastically deformed and containing several impurities [6]. On the other hand, synthetic chemical vapour deposited (CVD) diamond suffers less often from defects originating from plastic deformation. However, vacancy type defects are more commonplace in CVD diamond. In the following, the most common defect types in natural and synthetic diamond are described and their influence on the optical properties of diamond are discussed. Some of the defects occur naturally, while others are irradiation-induced.

Nitrogen is the most abundant impurity in diamond. Nitrogen can appear in very high concentrations, approaching 2500 atomic ppm (close to 1% of the diamond mass) [16]. Nitrogen can appear individually or as aggregates, and can form complexes with vacancies. The activation energy of nitrogen is so high that it has no practical importance as a n-type dopant in diamond electronics: for example, for a single substitutional nitrogen, $E_a = 1.7$ eV below the conduction band edge [17].

Diamond classification is based on whether the sample shows light absorption features related to nitrogen. Type I has a high concentration of nitrogen that causes absorption, whereas type II is lean on nitrogen with no nitrogen related absorption features present. Nitrogen-related centers are discussed in detail in, e.g., Refs. [18, 19]. Some of the typical defects and their positions in the gap are shown in figure 2.3. In type I natural diamond the most common nitrogen-related defect is the A aggregate, consisting of two substitutional N

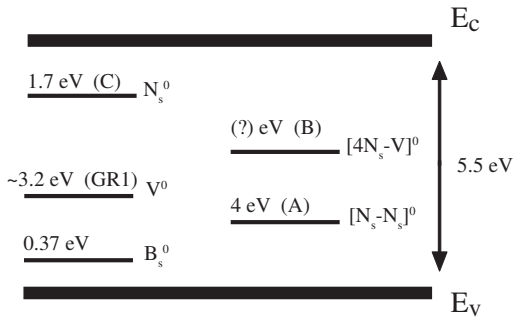

Figure 2.3. Band gap of diamond, with energy levels of different naturally occurring or irradiation-induced defect levels shown. The structure is shown on the righthand side of the defect level. A label is shown in parenthesis. The energy level values refer to the distance from the conduction band edge, expect for B_s^0 the distance is relative to valence band edge. The exact energy level of the B-centre is unknown.

atoms next to each other. The A aggregate causes absorption in the infrared (IR) and UV regions. The B centre most likely consists of a vacancy decorated by four nitrogen atoms [20]. Also the B centre causes absorption in the IR and UV regions. Some of the defects that absorb visible light include the C centre and the N3 centre. The C centre consists of a single substitutional N atom acting as a deep donor at 1.7 eV, absorbing light in the blue part of the visible spectrum. This results in a yellow colour. The N3 centre consists of a vacancy surrounded by three N atoms. The defect has been identified using electron paramagnetic resonance (EPR) experiments [21]. The N3 centre also causes yellowish colour. Of the non-nitrogen related naturally occurring impurities, boron is the most important. Boron is an acceptor with an energy level 0.37 eV above the valence band edge [22], meaning that it can be thermally ionized at room temperature to some degree. Boron-doped p-type diamond is blue.

One of the defects in diamond that has gained considerable interest recently is the vacancy-nitrogen pair, the N-V centre. The N-V centre occurs in two charge states, $[N\text{-}V]^0$ and $[N\text{-}V]^-$. The importance of the $[N\text{-}V]^-$ lies in its possible utilisation as a qubit in quantum computing. $[N\text{-}V]^-$features total spin $S = 1$, meaning that the magnetic spin number is $m_s = 0, \pm 1$. The long coherence time [23] and the possibility to manipulate and read the quantum state via EPR or optical spectroscopy makes it a potential qubit candidate [24]. This centre can occur naturally in diamond or it can be produced artificially by N^+-implantation [25] or, in nitrogen-containing diamond, by irradiation and subsequent annealing.

A big portion of natural diamonds have undergone plastic deformation that gives rise to extended defects. One of the features occurring together with the extended defects is the brown colour of natural type IIa diamond. Examples of

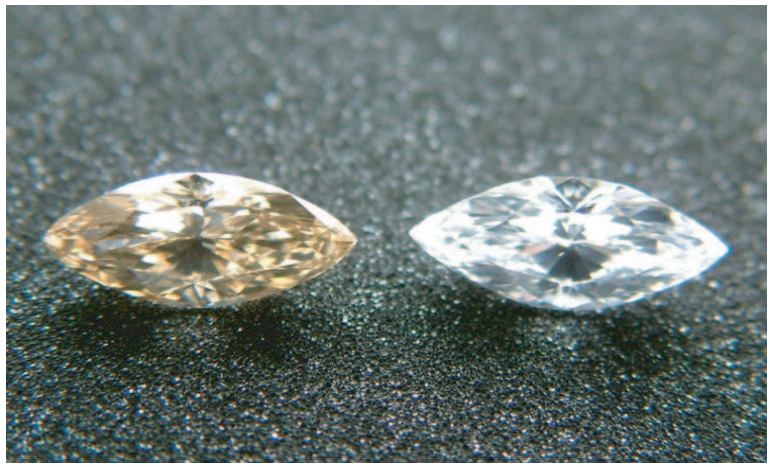

Figure 2.4. Examples of natural brown and transparent diamonds. Figure courtesy of Diamond Trading Company.

brown and transparent type IIa natural diamonds are shown in figure 2.4. The brown colour is caused by a featureless absorption ramp beginning at 2.0 eV (600 nm) (example of this is shown in figure 4.3). However, the origin of brown colouration in natural type IIa diamond (high purity, less than 10^{16} cm^{-3} of nitrogen or other impurities present) has evaded identification for long [26]. Recent advances in high temperature, high pressure treatments have brought new insight to the brown diamond problem [27, 28]. The brown colour gradually disappears during HPHT treatment when the temperature and pressure exceed 2000°C and 70 Mbar, respectively, suggesting that also the defects causing the colouration should disappear.

The continuous absorption suggests that there is a continuum of states in the band gap, making it improbable that the defect in question would be a simple point defect. It is known that the brown colour is related to the plastic deformation of the diamond crystal, since every brown natural type IIa diamond has undergone plastic deformation [29]. However, not all the plastically deformed diamonds are brown. Earlier it was thought that the brown colour is caused by dislocations. However, according to calculations, the density of optically active dislocations present in diamond is too low to cause the colouration [30]. Further, the density of optically active dislocations is not affected by HPHT treatment [31]. The first hints of the influence of the vacancy clusters on the brown colour were provided by positron annihilation measurements [32]. The measurements showed a large concentration of vacancy clusters present in brown type IIa diamond. The concentration of clusters reduced drastically during HPHT treatment in correlation with the reduction of the brown colour.

In addition, transmission electron microscopy (TEM) and electron energy loss spectroscopy (EELS) measurements [33, 34, 35, 36] have provided evidence of a correlation between the brown colour and vacancy clusters. Additionally, theory [37, 38, 39, 40, 41] suggests that large vacancy clusters in diamond are stable and can cause the brown colouration.

2.2 Aluminium nitride

AlN is thermodynamically stable in hexagonal wurtzite phase. AlN has a density of 3.26 g/cm^3, a lattice constant of a = 3.11 Å (ratio of lattice constants c/a=1.63), a thermal conductivity 285 W cm^{-1}K^{-1}, and a direct band gap of 6.2 eV [1]. As previously mentioned, the extreme mechanical, thermal, and electronic properties of AlN are results of the very tightly packed crystal structure with short bond lengths.

Being a member of the III-nitride family, AlN is a promising candidate for deep UV optoelectronic device. However, the doping of AlN has proven to be difficult. AlN can be alloyed with other nitrides in order to tailor the active wavelength of the optoelectronic device from infrared to ultraviolet regions. Additionally, AlN is an attractive choice as a substrate material for III-nitrides due to its good thermal conductivity and high electrical resistivity. Growth of thin film and bulk AlN has recently taken strides forward but still the material contains impurities and has less than ideal structural quality and optical properties. Problems related to vacancies include the compensation of intentional doping, absorption of the UV light [42] and the decrease of thermal conductivity [43]. The latter two play a role especially in the use of AlN as a substrate.

Lattice mismatch between the substrate and the active layer of an optoelectronic devices causes unwanted defects. In order to realise the full potential of III-nitride based optoelectronic devices, lattice matched substrates have to be developed. These can be either true bulk crystals or very thick heteroepitaxial layers that can be separated from the substrate. Physical vapour deposition (PVT) has emerged as a promising candidate for synthesising bulk crystals [44, 45, 46, 47]. Large substrates can be grown with relative ease compared to GaN and especially InN [48, 49]. This is due to the fact that the equilibrium N_2 pressure at the growth temperature is much lower in the case of AlN compared to other nitrides[50], enabling the use of sublimation methods [51], for example.

The sublimation growth of AlN is based on a sublimating a powder AlN source at a high temperature [52]. The precursor gases Al and N_2 react on the sur-

face of the seed (preferably a native AlN seed), forming single crystal AlN. The growth is driven by a temperature difference between the seed and the source. Vapour-phase Al is highly volatile at the growth temperatures in the proximity of 2500 K, requiring a high-purity seed and inert crucible walls. Despite the best of efforts, high concentrations of impurities, most notably O and C, are incorporated in the AlN single crystals. O and C are highly unwanted as they can hinder the control of electrical and optical properties, and cause additional crystallographic defects, such as vacancies.

2.2.1 Defects in AlN

Most of the research on the defects in AlN has been conducted using photo- or catholuminescence [53, 54, 55] or ab-initio calculations [56, 57, 58, 59, 60]. There exist a few reports employing positron annihilation [61, 62]. The experimental research of the defects in AlN is generally hampered by the rather poor crystalline quality of the sample material, caused by the efficient incorporation of impurities such as O. Thus, it is no surprise that catholuminescence (CL) and photoluminescence (PL) reports show a very prominent DX emission, most probably related to O and Si impurities [54, 55]. Considering vacancy type defects, based on experiments and theoretical calculations, it is generally accepted that the energy level of the N vacancy is at 5.87 eV above the valence band edge, rather close to the conduction band edge (the band gap is 6.13 eV) [53, 56, 58]. The exact energy level of the Al vacancy has not been established, but calculations suggests that it is in the region of 2.0-2.5 [58, 59]. The work on the Al vacancy in AlN presented in this thesis provides new information on the structure and energy levels of V_{Al} in AlN.

2.3 Optical properties and carrier dynamics of point defects

Point defects have a big influence on the optical properties of semiconductors, being able to act as recombination and generation centres. If a semiconductor sample is illuminated with sub-band gap light, charge carriers can be excited to defect states in the band gap. This results in optical absorption and possibly photo-conductivity [63]. The excitation and trapping of charge carriers to vacancies, i.e. charge-transfer processes, can be studied using positron annihilation spectroscopy, as positron trapping is sensitive to the charge state of a defect.

Non-equilibrium excess charge carriers can be generated, for example, by op-

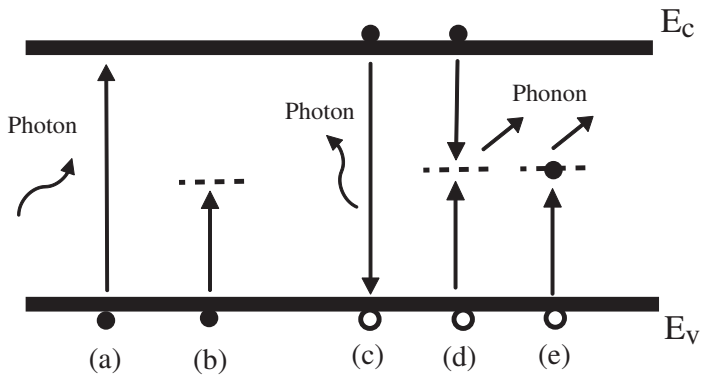

Figure 2.5. Different absorption and recombination mechanisms in semiconductors: (a) intrinsic and (b) extrinsic absorption, (c) band-to-band recombination, (d) trap-assisted recombination and (e) recombination from a trap.

tical absorption or by carrier injection [64, 65, 66]. A schematic presentation of different absorption and recombination processes is given in figure 2.5. Absorption and recombination processes involving electrons are discussed here, however, similar concepts apply also for holes. In absorption an electron is excited to a higher lying energy level, leaving behind a hole. In intrinsic absorption (a) an electron is excited to the valence band, whereas in extrinsic absorption (b) an electron is excited to a defect level in the band gap. By neglecting reflection, the intensity of photon flux can be written as

$$I = I_0 \exp(-\alpha x), \tag{2.1}$$

where I_0 is the original intensity, α is the absorption coefficient, and x the distance traveled by the photon in the medium. In the case of extrinsic absorption, α can be written in the form $\alpha = \sigma_{abs} N_d$, where σ_{abs} is the absorption cross section of the defect and N_d the density of the defects causing the absorption.

After absorption the electron lives in non-equilibrium in the conduction band or in a defect state until recombining with a hole. The recombination can be a direct band-to-band recombination (c) or trap-assisted (d), also called Shockey-Read-Hall, recombination. In indirect band gap semiconductors a direct recombination requires an involvement of a phonon, thus it is rather slow. In the case of direct band gap semiconductors the recombination is usually direct. Direct recombination is most often radiative, i.e., a photon is emitted, whereas trap-assisted recombination is often non-radiative, and the energy is dissipated as lattice vibrations. If an electron is trapped to a defect, the recombination can be modelled as a hole capture (e). The capture rate of holes is given by

$$g = \sigma_r \langle v_{th} \rangle p N_d^-, \tag{2.2}$$

where σ_r is the capture cross section, $\langle v_{th} \rangle$ is the thermal velocity of holes, p is the hole concentration and N_d^- is the density defects that have trapped an electron. There are several other physical mechanisms of recombination, e.g., cascade capture [67] and Auger capture [68].

Generally the time dependence of carrier generation-recombination process for electrons can be written as

$$\frac{dn}{dt} = G - \frac{n}{\tau}, \tag{2.3}$$

where n is the density of excited electrons, G the generation rate per unit time and τ the time constant of recombination. The model assumes, that the transition rate back to the ground is constant. After switching on the generation, a steady state is eventually achieved. In the steady state ($\frac{dn}{dt} = 0$), the density of excited electrons is constant $n = G\tau$. When the excitation is switched off (G=0), the time dependence of the electron density follows the relation

$$n = n_0 \exp(-t/\tau), \tag{2.4}$$

where n_0 is the electron density in the steady state. The excitation and recombination processes can be either direct between the bands or may involve one or more defect levels in the band gap. Similar equations hold for transitions involving holes.

When optical methods are used to study charge transfer processes involving vacancies, the concentrations vacancies in different charge states can be treated instead of electron or hole densities. In analogy to equation 2.3, the time dependence of vacancy concentration can be written as

$$\frac{d[V^-]}{dt} = \sigma_{abs}\phi[V^0] - g[V^-], \tag{2.5}$$

where $[V^0]$ and $[V^-]$ are the concentrations of a particular vacancy-type defect in neutral and negative charge states, respectively, ϕ is the photon flux, σ_{abs} the optical absorption cross section, and g transition rate back to the ground state ($g = \tau^{-1}$). The concentration of vacancies can be written as $[V^0_{dark}] = [V^0] + [V^-]$. Thus, the fraction of negative vacancies in steady state can be solved as

$$\frac{[V^-]}{[V^0_{dark}]} = \frac{\phi}{\phi + g/\sigma_{abs}}. \tag{2.6}$$

The decay rate g can be studied by switching off the illumination. Based on equation 2.2 the decay rate of electrons, i.e., the hole capture rate, can be written as

$$g = \sigma_p \langle v_p \rangle p[V^-]. \tag{2.7}$$

When the equilibrium hole concentration is high compared to the photogenerated hole concentration, decay rate g is simply constant. If it is assumed that there are no thermal holes present and that each electron excitation leaves a hole to the valence band, the hole concentration and the negative vacancy concentration are equal. The time dependence of the negative vacancy concentration can then be written as

$$\frac{d[V^-]}{dt} = \sigma_p \langle v_p \rangle [V_s^-]^2, \tag{2.8}$$

which can be solved for the negative vacancy concentration as

$$[V^-](t) = \frac{[V_s^-]}{\sigma_p \langle v_p \rangle [V_s^-]t + 1}. \tag{2.9}$$

Here $[V_s^-]$ is the concentration of negative vacancies in the steady state.

2.4 Semiconductor characterisation techniques

The methods that can be used to characterise vacancy-type defects in semiconductors can be divided into three classes: optical methods, electrical methods, and other methods, for example positron annihilation or electron paramagnetic resonance (EPR). Optical charaterisation techniques include, for example optical absorption spectroscopy, ellipsometry, and luminescence methods. Typical electrical methods include, e.g., deep level transient spectroscopy (DLTS) and Hall effect measurement. Naturally, different methods can be used to complement each other. For example, DLTS can be used to estimate charge carrier trap concentrations very efficiently, but the structure of the defects can not be resolved. In contrast EPR and positron measurements can provide information about the structure. All these methods can be used to obtain information about the optical properties of defects, either directly or indirectly. EPR, positron measurements, and many of the electrical methods can be combined with optical illumination to study the effect of light on defects. In the following some of the characterisation techniques are presented. Positron annihilation spectroscopy will be presented in detail in the next section.

On of the simplest of the characterisation techniques, in principle at least, is optical absorption spectroscopy. In absorption spectroscopy, monochromatic light is directed on a sample and the intensity of the light that is not absorbed is measured. Absorption spectroscopy can be used to obtain the concentration of the absorbing defects very conveniently if the absorption cross section is known.

Especially shallow defects are very efficiently detected [64]. When absorption is measured as a function of photon energy, the transition between two energy levels will result in an absorption peak and possibly a vibrational side band. Several defects in diamond are detected in this way.

Luminescence methods are based on the emission of photons due to recombination [69]. The initial generation of electron-hole pairs can be achieved optically (photoluminescence (PL)), by an electron beam (catholuminescence (CL)) or thermally (thermoluminescence (TL)). Luminescence methods are most suitable for studying shallow defects, as radiative recombination is required in order to detect the defect. Luminescence methods are also very sensitive; in favourable conditions even single luminescent centres can be detected [70]. However, obtaining the defect concentrations is more difficult. Luminescence properties are important in optoelectronic use; the intensity of excitonic emission (the emission of the bound state of an electron and a hole) is proportional to the optical quality at least when it comes to LEDs. Excitonic emission can occur due to recombination of free excitons (FE), or bound excitons (BE), or recombination through a donor-acceptor pair (D-A). Of these processes, the FE emission has the shortest wavelength and the D-A emission the longest.

Light can be used to manipulate the charge state of vacancies in order to obtain information about optical processes. Examples of this approach include optical EPR and optical DLTS (ODLTS). EPR measurements are based on the fact that unpaired electrons (in a vacancy, ion, or molecule, for example) absorb microwave radiation in a magnetic field when the energy corresponds to the Zeeman splitting of the electron levels. The fact that only unpaired electrons are detected makes EPR a very specific method. Illumination can be used to manipulate the charge state of a vacancy, making the defect either visible or invisible in EPR. However, EPR is limited to studying not too conductive bulk crystals, and defect concentrations are difficult to estimate. DLTS, in turn, is one of the most commonly used semiconductor charaterisation techniques [71]. In DLTS, charge carrier traps in the depletion region of a semiconductor are filled by a voltage pulse. After the pulse, thermal emission of charge carriers from the traps is detected by measuring capacitance. DLTS measurements are performed as a function of temperature. Different defects are detected via their activation energies. DLTS provides information on the concentration and on the carrier capture cross section of the defect. DLTS is a very sensitive, but very conductive or very insulating materials cannot be studied. DLTS requires efficient carrier injection. Thus conventional DLTS cannot be applied in the study of wide-bandgap semiconductors. However, electron-hole pairs can be

generated using optical excitation [72].

3. Positron annihilation spectroscopy

Positron annihilation can be used to study vacancy defects in semiconductors. It can provide information about the size, charge state, concentration, and chemical surrounding of vacancy defects. The method is based on the fact that the positron is the antiparticle of the electron and it will annihilate in matter. A positron will be driven to a negative or a neutral vacancy due to the Coulombic force caused by the ion cores. The positron lifetime and the energy distribution of annihilation radiation provides information about the annihilation site. The decreased electron density in a vacancy increases the positron lifetime and narrows the energy distribution of annihilation radiation.

3.1 Positrons in solids; diffusion and trapping

The life of a positron in matter can be divided to a few distinct phases: (i) implantation and fast thermalisation, (ii) thermal diffusion in the lattice, (iii) possible trapping to a lattice defect and (iv) annihilation either in a free state in the lattice or as bound to a defect. Positrons can be obtained from β^+ active isotopes or from pair production [7]. The most common isotope used in positron annihilation studies is ^{22}Na, an isotope of sodium with a half-life of 2.6 years. In the β^+ decay a proton of the nucleus is converted into a neutron, resulting in an emission of a positron and a neutrino. The resulting ^{22}Ne is in an excited state that decays in some picoseconds, and a 1.27 MeV gamma quantum is emitted. The emitted positrons have a continuous spectrum of kinetic energy up to 540 keV, meaning that the positrons originating from ^{22}Na probe the bulk of a sample. In order to study thin films and near-surface regions, positrons have to be first monochromated and then accelerated to a well defined energy. This can be achieved with a slow positron beam.

An implanted positron loses its kinetic energy very rapidly in a few picoseconds via ionisation, electron-hole excitation, and phonon emission. The time re-

quired for a positron to thermalise is negligible compared to the typical positron lifetime of 100-300 ps. A thermal positron diffuses in the material until it either annihilates in a free state or gets trapped to a lattice defect. Defects that can trap a positron include negative and neutral vacancies and negative ions. The trapping rate to a defect, i.e., the transition rate from a free state to a bound state is defined as

$$\kappa = \mu_D c_D, \tag{3.1}$$

where μ_D is the trapping coefficient, and c_D is the concentration of the defect. The trapping coefficient depends on the size, charge state, and ionic structure of the defect. For neutral monovacancies the trapping coefficient is typically in the range of $\mu_{V^0} = 10^{14} - 10^{15}$ s^{-1} whereas negative vacancies have trapping rates in the range of $\mu_{V^-} = 10^{15} - 10^{16}$ s^{-1} at room temperature [73, 74]. The trapping coefficient to negative vacancies is temperature sensitive, having $T^{-1/2}$ dependence [75].

There are two distinct phases in positron trapping: the diffusion to the defect and the subsequent quantum-mechanical transition from the free Bloch state to a localised bound state. If the defect concentration is small and the size of the defect is large, the time required for the positron to diffuse to the defect limits the trapping rate, i.e., trapping is diffusion limited. This is relevant for large clusters of vacancies and, e.g., dislocations. In the case of higher defect concentration, the trapping is limited by the quantum-mechanical transition rate to a bound state at the defect, i.e. the trapping is transition limited. If the trapping to a defect is transition limited, measurement as a function of temperature provides information about the charge state. Neutral defects show no temperature dependence, whereas trapping to negative defects increases strongly at low temperatures. Usually, neutral monovacancies can be detected if their concentration is at least 10^{16} cm^{-3}, and negative vacancies when the concentration is 10^{15} cm^{-3} or more. Vacancy clusters can be detected in somewhat smaller concentrations, since they trap positrons more efficiently than monovacancies. In addition, positrons can get trapped at negative ions, e.g, impurities, interstitials, antisites. The Coulomb attraction of negative ions produces shallow levels where positrons can be trapped. The binding energy for positrons in such defects is typically in the range of 10-100 meV, much lower than the typical value of around 1 eV for vacancies. Phonon-assisted escape from the shallow states, also called Rydberg states, occurs at temperatures above 50 K, and in some cases (depending on the binding energy) full detrapping requires temperatures as high as 800 K. When the escape rate is high, positrons do not annihilate

bound to negative ions anymore. The escape rate for a positron from a Rydberg state can be written as

$$\delta_{Ry} = \mu_{Ry}(\frac{2\pi m_+ k_B T}{h^2})^{3/2} \exp(-\frac{E_{b,Ry}}{k_B T}), \tag{3.2}$$

where $\mu_{Ry} = \mu_{R0} T^{-1/2}$ is the positron trapping coefficient from the delocalized state to a Rydberg state, m_+ the positron effective mass, and $E_{b,Ry}$ the binding energy to a Rydberg state.

Negative vacancies can also form shallow Rydberg states, which enhance the trapping rate at low temperatures. In this case the trapping is a two-step process [76], where a shallow Rydberg state acts as a precursor for the final transition to the bound state. In this case, the trapping coefficient is given by

$$\mu_V(T) = \frac{\mu_{Ry}}{1 + \frac{\mu_{Ry}}{\eta_R N_{at}} \left(\frac{m_+ k_B T}{2\pi\hbar^2}\right)^{3/2} e^{-E_{b,Ry}/k_B T}}, \tag{3.3}$$

where $\mu_{Ry} = \mu_{R0} T^{-1/2}$ is the positron trapping coefficient from the delocalized state to a Rydberg state, and N_{at} is the atomic density of the sample material.

In the case of a small concentration of extended defects, such as vacancy clusters or dislocations, the trapping can be diffusion limited. This is the case when the distance between the defects is of the same order as the diffusion length L_+. The trapping coefficient for spherical, homogeneously distributed vacancy clusters is then given by [9]

$$\mu = 4\pi r_d D_+, \tag{3.4}$$

where r_d is the radius of the vacancy cluster, and the positron diffusion coefficient $D_+ \propto T^{-1/2}$ below 500 K. The temperature dependence is due to scattering off longitudal acoustic phonons. If neither diffusion nor transition limited trapping dominates, the inverse of the total trapping coefficient can be written as

$$\frac{1}{\mu_D} = \frac{1}{\mu_{diff}} + \frac{1}{\mu_{trans}}. \tag{3.5}$$

3.2 Kinetic equations

The time-dependent behaviour of positrons in the crystal lattice can be modeled using the kinetic equations [9]

$$\frac{dn_B}{dt} = -(\lambda_B + \sum_{j=1}^{N} \kappa_{Dj}) n_B + \sum_{j=1}^{N} \delta_{Dj} n_{Dj}, \tag{3.6}$$

$$\frac{dn_{Dj}}{dt} = \kappa_{Dj} n_B - (\lambda_{Dj} + \delta_{Dj}) n_{Dj}, \tag{3.7}$$

where λ is the annihilation rate, κ is the trapping rate to a defect, δ_{Dj} is the detrapping rate, and the subscripts B and Dj refer to the delocalised state and to a defect j, respectivily. In the kinetic equations it is assumed that (i) at time $t = 0$ the positron is in the delocalized state, (ii) the trapping rate is proportional to the defect concentration, and (iii) the positron can escape from some of the traps. Assumption (i) results in the boundary conditions

$$n_B(0) = 1, n_{Dj}(0) = 0. \tag{3.8}$$

From the kinetic equations the probability that the positron has not annihilated at time t can be written as

$$n(t) = n_b(t) + \sum_{j=1}^{N} n_{Dj}(t) = \sum_{i=1}^{N+1} I_i \exp(-\lambda_i t), \tag{3.9}$$

where λ_i is the decay constant and I_i is the corresponding relative intensity. The largest λ_i corresponds to annihilations in the delocalised state in the lattice combined with the transition rate to the bound states at defects. The other values of λ_i correspond to the values of λ_{Dj} directly.

Based on equation 3.9, the experimental positron lifetime spectrum can be written as

$$-\frac{dn(t)}{dt} = \sum_{i=1}^{N+1} I_i \lambda_i \exp(-\lambda_i t). \tag{3.10}$$

The inverse of the decay constant is the characteristic positron lifetime in the state i, $\tau_i = 1/\lambda_i$, called the positron lifetime component. The annihilation fraction η_j is the probability for the positron to annihilate in the state j. Thus,

$$\eta_B = \int_0^\infty dt \lambda_B n_B(t) = \lambda_B n_B^*, \tag{3.11}$$

and

$$\eta_{Dj} = \int_0^\infty dt \lambda_{Dj} n_{Dj}(t) = \lambda_{Dj} n_{Dj}^*, \tag{3.12}$$

where $n_i^* = \int dt n_i(t)$. The time-integrated probabilities can be solved from equations (3.6-3.7) and with the boundary conditions (3.8)

$$(\lambda_B + \sum \kappa_j) n_B^* + \sum \delta_j n_{Dj}^* - 1 = 0, \tag{3.13}$$

$$\kappa_j n_B^* - (\lambda_{Dj} + \delta_j) n_{Dj}^* = 0. \tag{3.14}$$

The annihilation fractions are solved from equations (3.13 - 3.14), i.e.,

$$\eta_B = \frac{\lambda_B}{\lambda_B + \sum_{j'} \frac{\kappa_{Dj'}}{1+\epsilon_{Dj'}}}, \tag{3.15}$$

$$\eta_{Dj} = \frac{\kappa_{Dj}}{(1+\epsilon_{Dj}) + (\lambda_B + \sum_{j'} \frac{\kappa_{Dj'}}{1+\epsilon_{Dj'}})}, \tag{3.16}$$

where $\epsilon_{Dj} = \delta_{Dj}/\lambda_{Dj}$ is the positron detrapping ratio from the trap j.

Starting from the kinetic equations 3.6 and 3.7, the trapping rates can be estimated from the experimental data in certain cases. When there is one defect type present and no detrapping occurs, using boundary conditions $n_b(0) = 1$ and $n_D(0) = 0$ the trapping rate can be solved as

$$\kappa = \frac{1}{\tau_B} \frac{\tau_{ave} - \tau_B}{\tau_D - \tau_{ave}}. \tag{3.17}$$

When there are two types of defects present, the trapping rate can be solved only in some special cases. If it is assumed that the positrons annihilate in three different states, of which the two shorter components are mixed (i.e., they cannot be separated from the experimental spectrum) and the longest component is experimentally well separated, the trapping rates can be written as [9]

$$\kappa_1 = \frac{\tau_{1,exp}(\lambda_B - I_{2,exp}\lambda_{D2}) - I_{1,exp}}{\tau_{D1} - \tau_{1,exp}}, \tag{3.18}$$

and

$$\kappa_2 = \frac{I_{2,exp}}{I_{1,exp}}(\lambda_B - \lambda_{D2} + \kappa_1). \tag{3.19}$$

This is the situation when there are at the same time vacancies, and bigger vacancy clusters and part of the positrons annihilate in the delocalised state.

If the trapping rate to the defects is much faster than the positron annihilation in the bulk, i.e., $\kappa_{1,2} >> \lambda_B - \lambda_{D1,2}$, positron trapping is in saturation. No free positrons are detected and the sensitivity to defect concentration is lost. However, then the relative trapping rate can still be estimated as

$$\frac{\kappa_2}{\kappa_1} = \frac{I_2}{I_1}. \tag{3.20}$$

3.2.1 Experimental and theoretical techniques

Experimental positron techniques include positron lifetime spectroscopy and the methods based on measuring the energy of the annihilation radiation, such as Doppler broadening spectroscopy. The same trapping kinetics are valid for both of these methods. The measurable parameter, be it the average positron lifetime τ_{ave} or the Doppler broadening parameters S or W, is the weighted sum over all positron states

$$A = \eta_B A_B + \sum_j \eta_{Dj} A_{Dj}. \tag{3.21}$$

Positron lifetime measurement

The positron lifetime can be measured by detecting the time difference between the start signal and one of the two 511 keV annihilation photons. In the case of a ^{22}Na source the start signal is provided by the 1.27 MeV photon emitted nearly simultaneously with the positron. The lifetime events are stored into a histogram, called the lifetime spectrum. An ideal lifetime spectrum is of the form of equation 3.10. In practice, the ideal spectrum is convoluted with the Gaussian timing resolution of the measurement setup. Typically the full width at half maximum (FWHM) of the setup is of the order of 250 ps. The lifetime components corresponding to different annihilation states can be fitted to the spectrum. Fitting is unambiguous if the different lifetime components are well separated, i.e., $\tau_1/\tau_2 > 1.5$. The average positron lifetime is then defined as

$$\tau_{ave} = I_B\tau_B + \sum_i I_{Di}\tau_{Di}. \tag{3.22}$$

Usually, the maximum number of components that can be fitted is three. The average lifetime can always be estimated, as it is the centre of the mass of the lifetime spectrum

$$\tau_{ave} = \int_0^\infty dt\ n(t) = \sum_i I_i\tau_i. \tag{3.23}$$

Doppler broadening measurements

Positron studies of thin films require slowing down the fast positrons to thermal energies. Hence, the start signal used in lifetime experiments is lost and the positron lifetime cannot be measured. However, the energy of the annihilation radiation is sensitive to the annihilation site and provides information about the vacancy content. High-purity Ge detectors, with typical energy resolutions in the range of 1.3-1.5 keV (FWHM) at 511 keV, are used. The momentum of distribution of electrons results in a broadening of the 511 keV annihilation line. The momentum of a thermal positrons is negligible and does not contribute to the Doppler broadening. The Doppler shift (to the first order) is then given by the equation

$$\Delta E = \frac{1}{2}cp_L, \tag{3.24}$$

where c is the speed of the light and $p_L$is the lateral momentum component of the annihilating electron. In practice the experimental Doppler spectrum can be written, assuming that there is only a single defect type present, as

$$\rho_{meas} = (1-\eta_V)\rho_B + \eta_V\rho_V, \tag{3.25}$$

where ρ_{meas} is the measured spectrum, ρ_B the spectrum of a defect free lattice, and ρ_V the vacancy specific spectrum.

Background in the high-momentum region can be strongly reduced by using two Ge-detectors in the coincidence mode, i.e., by requiring that both of the 511 keV annihilation photons are detected. The reduction of the peak-to-background ratio drastically improves the measurement accuracy in the high-momentum region, providing more information on the type of electrons annihilating. This enables the identification of the chemical surrounding of the annihilation site, as the high-electron-momentum region is characteristic to the outermost core electron shells of the atom [77]. This is extremely practical as the electron momentum distribution of different vacancy-impurity structures can be calculated theoretically [11], making direct comparison between experiment and theory possible. The coincidence-Doppler-broadening spectra are usually normalised to the defect-free lattice. These ratio curves show visually the characteristic features typical of decorating atoms.

Positron annihilation parameters theoretically

The positron annihilation parameters can be calculated theoretically starting from the one-particle Schrödinger equation for the positron ground state (Ψ_+, E_+)

$$-\frac{\hbar^2}{2m}\nabla^2\Psi_+(\boldsymbol{r}) + V(\boldsymbol{r})\Psi_+(\boldsymbol{r}) = E_+\Psi_+(\boldsymbol{r}), \tag{3.26}$$

where $V(\mathbf{r}) = V_{Coul}(\mathbf{r}) + V_{corr}(\mathbf{r})$. The first term is the Coulombic potential and the second term is the electron-positron correlation. The theoretical positron lifetime can then be calculated as

$$\frac{1}{\tau} = \pi r_0^2 c \int d\boldsymbol{r}|\Psi_+(\boldsymbol{r})|^2 n(\boldsymbol{r})\gamma[n(\boldsymbol{r})], \tag{3.27}$$

where r_0 is the classical radius of the electron, c the speed of light, $n(\mathbf{r})$ is the electron density and $\gamma[n]$ the enhancement factor of the electron density at the positron [10]. Based on equation 3.27 it can be understood that for large positron lifetimes the overlap between the electron and the positron must be small in all three dimensions. This means that line and planar defects have small positron lifetimes even though the total open volume of the defects might be very large.

Similarly, the calculated theoretical momentum distribution of the annihilation radiation can be compared to the experimental Doppler-broadening data. The theoretical momentum distribution of the annihilation radiation is written as

$$\rho(\boldsymbol{p}) = \frac{\pi r_0 c}{V}\sum_i \gamma_i \left| \int \mathrm{d}\boldsymbol{r} e^{-i\boldsymbol{p}\boldsymbol{r}} \psi_+(\boldsymbol{r})\psi_i(\boldsymbol{r}) \right|^2, \tag{3.28}$$

where V is the normalisation volume. The calculation of the annihilation momentum distribution requires the knowledge of occupied electron wave functions $\psi_-(\boldsymbol{r})$.

3.3 Studying the optical properties of vacancies using positron spectroscopy

3.3.1 A setup for positron measurements with optical illumination

In this thesis, a setup for measuring time-dependent optical properties of vacancies has been developed. The setup is based on high-power LEDs with quick switch-on times. The LEDs are controlled by a metal-oxide semiconductor field effect transistor (MOSFET). A schematic presentation of the setup is shown in figure 3.2. The LEDs are driven by 1.5 A maximum forward current. The high power of the LEDs, approaching 10 W, means that heat has to be dissipated. Therefore LEDs are mounted on copper holders, which can be additionally cooled by a fan. The transistor and a 10 Ω resistor are mounted on a heat sink. The measurement is controlled by a National Instruments Fieldpoint I/O module, a pulse generator, or a direct-voltage source. The MOSFET transistor, for example Phillips BLF244, can be controlled using voltages in the range of 0-10 V.

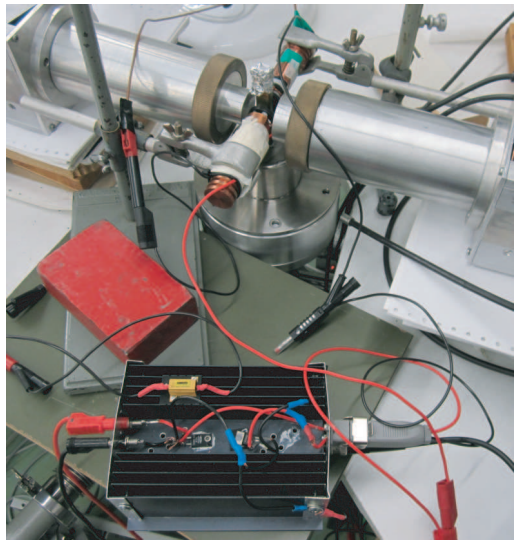

Figure 3.1. Part of the experimental setup used in optical positron measurements. The MOSFET is mounted on the black heat sink. The LEDs are mounted on the copper holders.

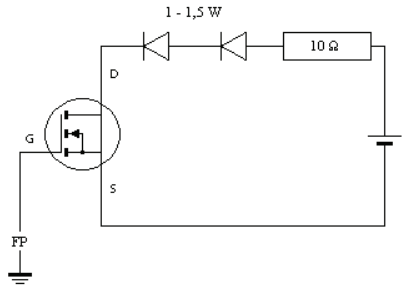

Figure 3.2. A schematic presentation of the setup.

The setup can be used to study photoinduced charge transfer processes of the vacancies. Measurements have been conducted in slots after a light pulse, as shown in figure 3.3. After a sufficient number of slots, high enough number that the optical effect has decayed, the loop is started all over. A typical measurement in the work presented in this thesis has 30 × 10 s slots and the measurements are looped at least 1000 times. The measurement is controlled by a National Instruments Labview-based program, which controls both the illumination (using Fieldpoint) and the collection of the annihilation events. A lifetime spectrum is obtained for each time slot.

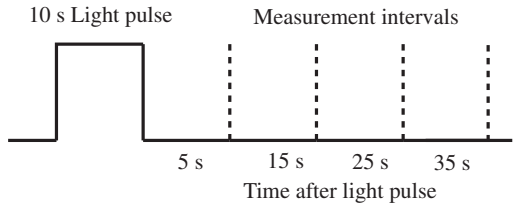

Figure 3.3. Positron lifetime spectrum is measured in slots after the light pulse. The measurements are repeated several hundred times in order to obtain sufficient number of annihilations.

3.3.2 Analysing the influence of optical excitation on the positron lifetime

As explained in section 2.3, optical illumination can be used to manipulate the charge state of a vacancy. There exist several reports exits on combining positron measurements with optical excitation [78, 79, 80, 81, 82]. The change of the charge state is detected as a change in the trapping rate. By varying the incident photon energy, the density of states induced by the defects can be studied. The measurements are comparable to the optical absorption measurements, as optical absorption is also proportional to the density of states.

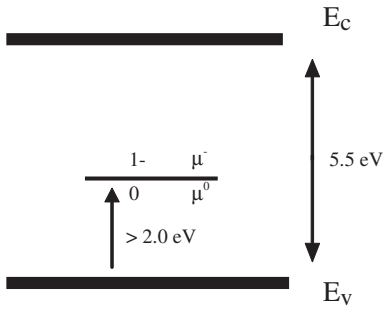

Figure 3.4. Illustration of the effect of photon excitation to the positron trapping in diamond. Below the ionisation level the defect is in neutral charge state and the trapping coefficient is μ^0. Above that the defect is negative and the trapping coefficient is μ^-.

However, it should be noted that in the case of positron measurements it is the ratio g/σ_{abs}, given by equation 2.6, that is actually measured. Thus, the effect seen by positrons depends not only on the absorption cross section σ_{abs}, but also on the decay rate g of the photoexcitation. If the decay is very rapid, the population of electrons in vacancies is small even with large absorption cross sections.

The effect of illumination can be studied by estimating the trapping rate (or the relative trapping rate) corresponding to the optically active defect. If the defect is neutral in the dark and negative under illumination, the trapping rate to the optically active defect κ_2 can be written as

$$\kappa_2 = \left(1 - \frac{[V^-]}{[V^0_{dark}]}\right)\kappa^0 + \frac{[V^-]}{[V^0_{dark}]}\kappa^-, \tag{3.29}$$

where $[V^-]$ is the concentration of negative vacancies, $[V^0_{dark}]$ the concentration of vacancies in the dark, κ^0 the trapping rate to a neutral vacancy, and κ^- the trapping rate to a negative vacancy. This is illustrated in figure 3.4. The fraction of vacancies in a negative charge state can be solved as

$$\frac{[V^-]}{[V^0_{dark}]} = \frac{\kappa_2 - \kappa^0}{\kappa^- - \kappa^0}. \tag{3.30}$$

In practice, estimating the absolute trapping rate is not always necessary, as only the relative change of the trapping rate can be of interest. It will be shown in chapter 5 that in the case of natural diamond, the trapping rate to the defect causing the shorter lifetime component is not optically active, i.e., κ_1 is constant under illumination. Thus, during flux- and time-dependent measurements, the sum $\lambda_B - \lambda_{D2} + \kappa_1$ of equation 3.19 is constant and the fraction of negative clusters can be written as

$$\frac{[V^-]}{[V^0_{dark}]} = \frac{I_2/I_1 - (I_2/I_1)^0}{(I_2/I_1)^- - (I_2/I_1)^0}, \tag{3.31}$$

where $(I_2/I_1)^0$ and $(I_2/I_1)^-$ are the ratios of experimental intensities for neutral and negative clusters, respectively.

4. Identifying the origin of brown colour in natural type IIa diamond

In this chapter the origin of brown colour in type IIa diamond is studied. Positron lifetime measurements show that there are vacancy clusters present in the brown diamond samples. Further, the vacancy clusters show optical activity when illuminated with sub-band gap monocromatic light. In order to obtain direct evidence on the influence of the vacancy clusters to the brown colour in type IIa diamond, a systematic study of the vacancy cluster concentration and optical absorption at different stages of HPHT anneal has been conducted. The brown diamond was originally 1.3 cm^3 in size. The diamond has been heat treated in four different stages, at temperatures 1860, 2080, 2300 and 2500 °C. After each annealing stage, a pair of roughly 5×5×0.5 mm^3 sample pieces were cut for positron and optical absorption measurements. During the annealing, the optical absorption of the samples gradually decreases. The samples are completely transparent after the last annealing stage.

4.1 Positron lifetime in brown and colourless type IIa diamond

Positron lifetime spectra for the brown samples and naturally colourless samples are shown in figure 4.1. The average lifetime of the brown sample is much longer than in the transparent sample, and the lifetime further increases when the sample is illuminated. The fitted average lifetimes and lifetime components, including corresponding intensities, are presented in table 4.1.

Table 4.1. Positron lifetime results at 20 K in the dark and with 3.0 eV illumination for the brown diamond and the HPHT treated (originally brown) colourless diamond.

Sample	τ_{ave} (ps)	τ_1 (ps)	τ_2 (ps)	I_2 (%)
Brown	164	125	405	12.2
HPHT colourless	122	118	340	2.5
Brown, 3.0 eV illumination	227	132	421	33.2

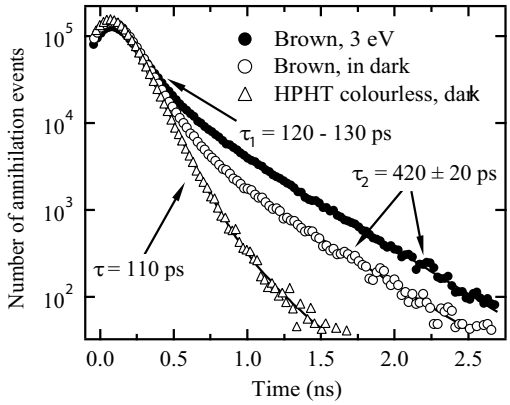

Figure 4.1. Experimental lifetime spectra for the transparent HPHT treated diamond sample and the brown diamond in the dark and with 3.0 eV photexcitation.

The measured average positron lifetimes are longer than that reported for annihilation in the diamond lattice, 100 ps [83]. This suggests that all the samples contain open-volume defects. The shortest fitted lifetime component is of the order of 110-120 ps in both the brown and the colourless diamonds. The reported positron lifetime in a diamond monovacancy is 145 ps [84, 85]. In the brown diamond there is additional second lifetime component of 420 ± 20 ps. The intensity of the 420 ps component further increases when the sample is illuminated with 3.0 eV light, as is clearly seen in figure 4.1.

4.2 Theoretical calculations

In order to identify the defects corresponding to the lifetime components theoretical calculations have been performed using the MIKADoppler program [86]. The positron lifetimes have been estimated for a defect free lattice, for dislocations of different types, for vacancies, and for vacancy clusters of size of up to 100 missing atoms. The positron lifetime the in diamond lattice given by MIKADoppler is 90 ps, 10 ps less than the reported experimental value for the defect free bulk. This is expected, since employed approximations tend to underestimate lifetimes. The theoretical positron lifetimes in different types of defects are listed in table 4.2.

An ideal monovacancy (no inward or outward relaxation) results in a positron lifetime of 96 ps, only 6 ps higher than the value in the defect-free diamond lattice. However, relaxing the nearest C atoms outward by 5 % results in a positron lifetime of 116 ps, and by relaxing the atoms further outward by 10 % results in a lifetime as high as 146 ps. Thus it can be concluded that in

Table 4.2. Theoretical (uncorrected) positron lifetimes for small open volume defects.

Defect type	Theoretical positron lifetime (ps)
Defect free lattice	90
Ideal monovacancy	96
Monovacancy with 5 % relaxation	116
Monovacancy with 10 % relaxation	146
Glide dislocation	96
Shuffle dislocation	129

order to obtain the reported positron lifetime of 145 ps for the monovacancy, the vacancy has to be relaxed outward by 5-10 %. Different dislocation structures [87] yield positron lifetimes comparable to those of monovacancies. Especially shuffle type dislocations contain a large open volume, resulting in a positron lifetime of 129 ps, whereas glide dislocations give a shorter lifetime of 96 ps. Due to the fact that the dislocation structures and monovacancies result in similar lifetime components, it is not possible to say whether the detected short lifetime component $\tau_1 = 115 - 132$ ps corresponds to positrons annihilating in dislocations or in monovacancies. However, the open volume of the defects in question must be comparable to that of the monovacancy.

Positron lifetimes for very large vacancy clusters have also been calculated. The sensitivity of the positron lifetime to the size of the vacancy cluster is very weak for lifetimes around 400 ps due to the fact that free positron lifetimes saturate at 500 ps. The number of missing atoms can be determined to the order of around 10 atoms. The calculated positron lifetime as a function of the number of missing atoms in the cluster is shown in figure 4.2. The structures for the smaller clusters (less than 20 missing atoms) were provided by L. Hounsome [88]. The atoms were removed in such an order that the number of dangling bonds was minimised. Larger clusters were obtained by removing atoms according to their proximity to the centre of the cluster. The relaxation of the cluster was omitted, since for large open volumes the effect of relaxation is negligible. Based on the calculations it can be concluded that the positron lifetime of 420 ± 20 ps corresponds to 40-60 missing atoms. The exact shapes of the vacancy clusters cannot be evaluated based on the positron measurements alone, but it is clear that it has to be a real three-dimensional open volume. There exists some evidence that the clusters could be spherical [35, 39, 40].

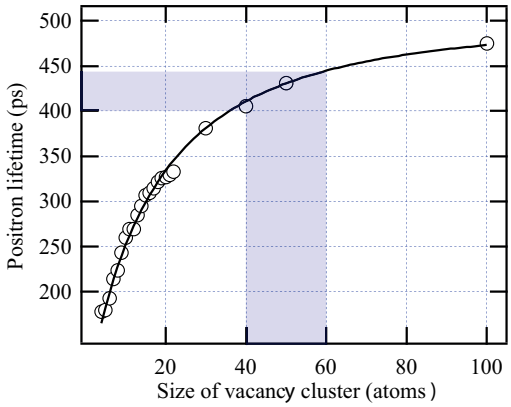

Figure 4.2. Theoretical positron lifetimes in vacancy clusters as a function of the number of missing atoms.

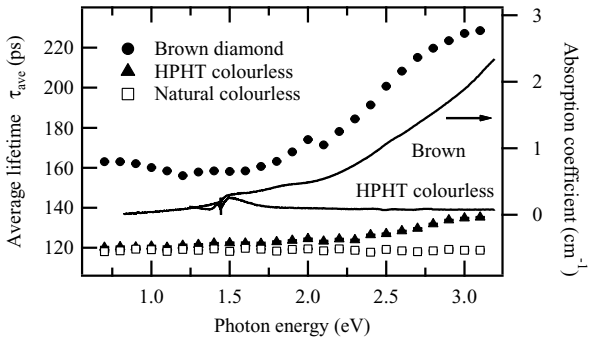

Figure 4.3. Average positron lifetime (left scale) for a brown, HPHT treated transparent and naturally transparent diamond as a function of photon energy. The absorption coefficient for brown and HPHT treated is shown on the right scale.

4.3 Effect of the photoexcitation on the positron lifetime

Positron lifetime has been measured under photoexcitation at 20 K with photon energies of 0.7-3.0 eV. The results are shown in figure 4.3. In brown diamond the average lifetimes increases monotonously with increasing photon energies. The absorption coefficient start to increase at similar energies. Results of HPHT colourless and naturally colourless samples have been plotted for comparison. There is some illumination effect present in the HPHT treated sample, suggesting that some optically active vacancy clusters persist after the anneal. The naturally colourless sample does not show any illumination effect. The lifetime component τ_1 is constant in all the samples through the whole energy range. τ_2 is also constant. It is interesting to note that in the brown diamond the average positron lifetime slightly decreases with photon energies of 1.0-1.7 eV, compared to the situation in the dark.

The intensity of the lifetime component $\tau_2 = 420 \pm 20$ ps behaves in a similar

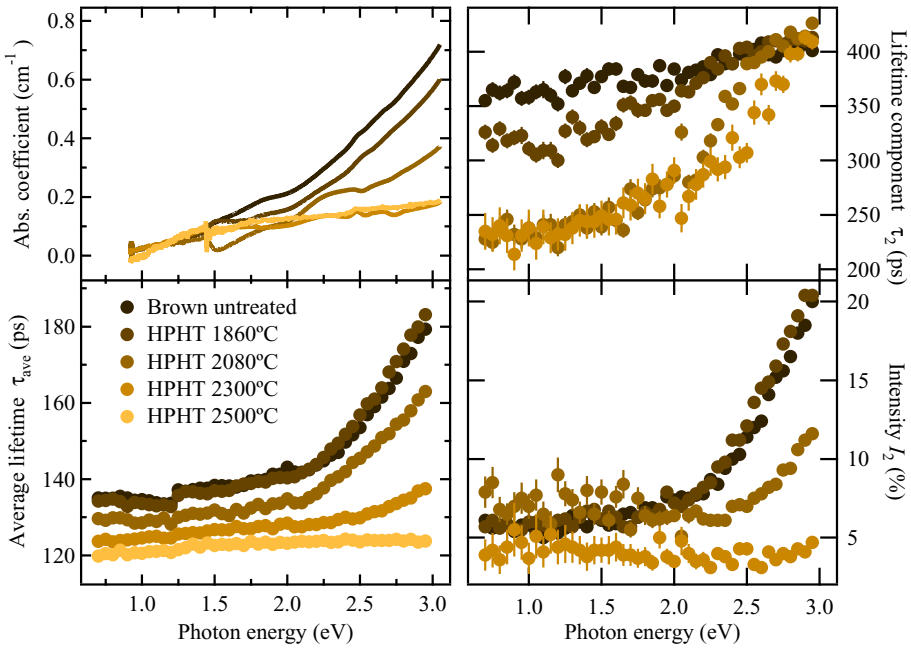

Figure 4.4. Optical absoprtion, average positron lifetime, lifetime component τ_2, and corresponding intensity as a function of photon energy.

manner as the average lifetime (not shown). It is clear that the increase of the average lifetime is due to increased trapping at the vacancy clusters. The most obvious reason for the enhanced trapping to the vacancy clusters is that the trapping coefficient corresponding to the vacancy clusters increases due to the negative charging of the cluster.

4.4 Effect of HTHP treatment on the vacancy content

The influence of HPHT treatments on the loss of optical absorption has been studied in detail with type IIa diamond plates cut from a one large diamond sample and isochronally (1 h) heat treated at 1860, 2080, 2300 and 2500°C. The positron lifetime and the optical absorption results are plotted in figure 4.4.

The broadband absorption decreases gradually during the treatment. In the first annealing stage at 1860°C the absorption is unaffected. At 2080°C the absorption has decreased considerably to roughly half of its original value. Finally, at and above 2300°C the absorption is close to that of the originally colourless samples. Also the positron lifetime decreases in a similar manner. By comparing the intensity of the second lifetime component to the optical absorption,

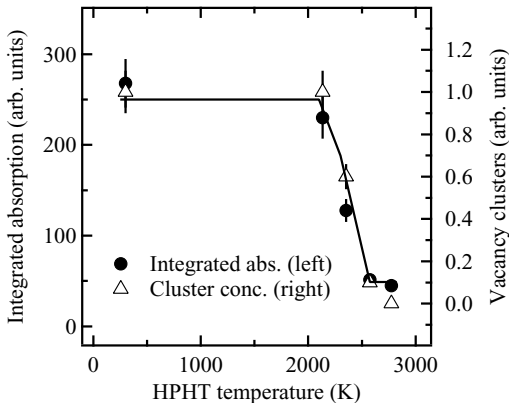

Figure 4.5. Relative cluster concentration and integrated absorption as a function of HPHT temperature.

the correlation is evident during all the HTHP stages: the higher the annihilation intensity at the vacancy clusters, the stronger the absorption at visible wavelengths. The shorter lifetime component (not shown) is constant between 120-125 ps in all the samples irrespective of the anneal stage or optical excitation.

In the HPHT treated samples the second lifetime component τ_2 gradually decreases to close to 250 ps as the treatment progresses. The value of τ_2 further decreases close to 230 ps when the samples are illuminated with photons of energy of the order of 1.0 eV. This suggests that the optical effect at 1.0-1.5 eV might be due to intermediate-sized defects with positron lifetime in the region of 200-250 ps. However, these defects do not seem to contribute to the optical absorption because the absorption is minimal below 2.0 eV.

The correlation between optical absorption and the vacancy cluster concentration can be studied in more detail by comparing the integrated optical absorption and the relative vacancy cluster concentration. The optical absorption has been integrated between energies 2.0-3.0 eV. The trapping rate to the vacancy clusters can be estimated using equation 3.19. However, the value of κ_1 is constant through all the anneal stages when the samples are in the dark. Thus, the trapping rate to the vacancy clusters can be written as $\kappa_2 = I_2/I_1 \times C$, where C is a constant. The vacancy cluster concentration, relative to the unannealed sample, can be calculated as $c_{rel} = \kappa_2^{annealed}/\kappa_2^{unannealed}$. The relative cluster concentration and the integrated absorption are shown in figure 4.5. The figure shows a strong correlation between the removal of the brown colour and the decrease of the vacancy cluster concentration.

In summary, the origin of brown colour in natural type IIa diamond can be attributed to vacancy clusters of 40-60 missing atoms, resulting in a positron

lifetime of 420 ± 20 ps. The evidence of this is twofold: (i) the positron trapping to the vacancy clusters shows a strong correlation with optical absorption as a function of photon energy, and (ii) the vacancy clusters disappear during the HPHT treatment in correlation with the removal of the brown colour. The optical effect is likely due to the negative charging of the vacancy clusters, resulting in the absorption of photons. When diamond is HPHT treated the clusters dissociate and the brown colour disappears.

5. Microscopic nature of the illumination effects in natural type IIa diamond

The nature of the charge transfer processes related to the photoexcitation of vacancy clusters in brown type IIa natural diamond has been studied using the transient illumination setup presented in section 3.3. The easily separated 400 ps lifetime component of the optically active vacancy cluster and the slow decay of the effect makes diamond an ideal starting point for developing the setup and models before studying more subtle effects. By combining the transient measurements with flux-dependent steady-state measurements, the optical absorption cross section and subsequently the vacancy cluster concentration can be estimated. The illumination model presented in section 2.3 suggests that free holes should be generated in photoexctitation. Photoconductivity measurements have been conducted in order to verify this.

Positron lifetime measurements have been conducted under photoexcitation in transient and steady-state modes in the temperature range of 45-300 K. The illumination is provided by LEDs at near-UV, blue, and green wavelengths. Specifications of the LEDs are shown in table 5.1. At 3.1 eV, the 700 mW radiant power corresponds to a photon flux of roughly $2 \times 10^{16}\mathrm{cm}^{-2}\mathrm{s}^{-1}$ on the sample, with the geometry used. This is considerably higher than $10^{14}\mathrm{cm}^{-2}\mathrm{s}^{-1}$ that was previously obtained using a halogen lamp.

Table 5.1. The specifications of the high-power LEDs used in the study.

Colour	Wavelength (nm)	Photon energy (eV)	Radiant power (mW)
Near-UV	400	3.1	700
Blue	465	2.7	970
Green	525	2.4	340

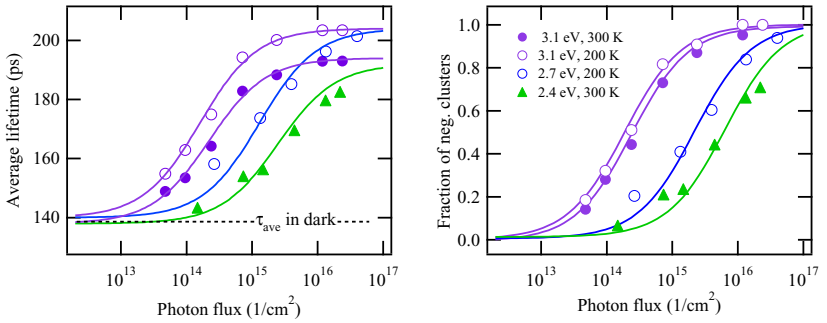

Figure 5.1. Average positron lifetime as a function of photon flux and the corresponding fraction of negative clusters estimated using equation 2.6. The measurement temperature and the photon energies are indicated.

5.1 Flux dependence of photoexcitation

The average positron lifetime measured as a function of photon flux is plotted in the left panel of figure 5.1. The measurements have been conducted at 200 or 300 K, since at lower temperatures the positron trapping approaches saturation. The average lifetime starts to increase with photon fluxes above $10^{13}\mathrm{cm}^{-2}\mathrm{s}^{-1}$ and saturates at fluxes above $10^{16}\mathrm{cm}^{-2}\mathrm{s}^{-1}$. The effect is essentially the same for energies of 3.1, 2.7 and 2.4 eV, although the photon flux emitted by the 2.4 eV LED does not seem to be high enough to cause saturation. The average lifetime increases because more vacancy clusters become negatively charged with increasing photon flux. The negative clusters have a higher trapping coefficient than the neutral ones, attracting positrons more efficiently. The saturation of the average lifetime can be attributed to the fact that all the vacancy clusters are in a negative charge state. However, the exact charge state of the clusters cannot be estimated, as the sensitivity between different negative charge states is much smaller than the difference between the neutral and negative charge states [10].

The fraction of negative vacancy clusters has been estimated using equation 3.31 and it is shown on the right panel of figure 5.1. The fits shown in the figure are based on equation 2.6. The fitted values of g/σ are shown in table 5.2. The fit matches the experimental data well. It should be noted that based on the flux-dependent measurements, the fitting parameter g/σ is constant as a function of the flux, suggesting that the parameter g is also constant as a function of the photon flux.

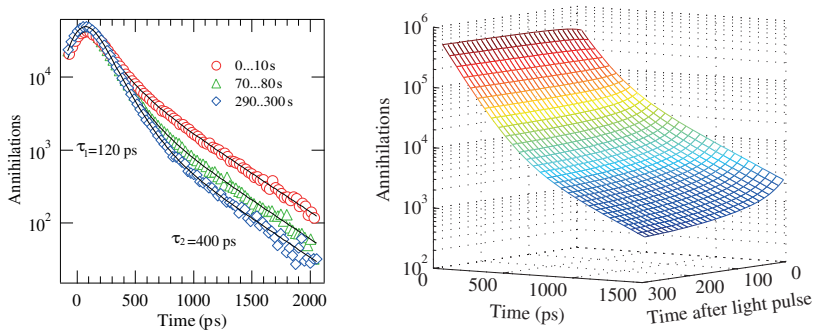

Figure 5.2. Positron lifetime spectra after a light pulse. On the left panel the lifetime spectrum is plotted for three measurement slots. The time after the light pulse indicated is indicated. From the figure it is clearly seen that the intensity of the 400 ps lifetime component decays. On the right panel, the time evolution of the lifetime spectrum after a light pulse is shown. Each time slot is 10 s.

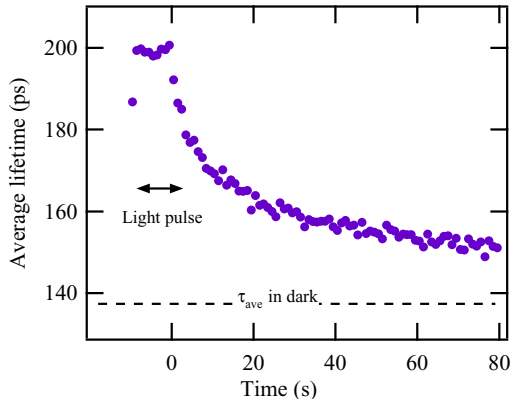

Figure 5.3. Average positron lifetime as a function of time during and after a 3.1 eV light pulse with a photon flux of $2\times10^{16}\mathrm{cm}^{-2}\mathrm{s}^{-1}$. A positron lifetime spectrum has been collected for each 1 s measurement point. After switching on the illumination, the average lifetime increases rapidly. The decay of the photoexcitation effect is much slower.

5.2 Transient effects

In order to obtain the value of the optical absorption cross section σ_{abs}, the decay rate g has to be determined. This can be done by studying the decay of the photoexcitation effect, using the setup presented in section 3.3. The positron lifetime has been measured in slots after switching off the illumination. A lifetime spectrum was collected for each measurement slot. At the photon energy 3.1 eV the measurement slot length was 10 s, while at 2.7 and 2.4 eV, 3 s slots were used, because the decay of the photoexcitation effect was more rapid. An example of the time evolution of the lifetime spectrum is shown in figure 5.2.

The average positron lifetime during the illumination cycle is plotted in figure

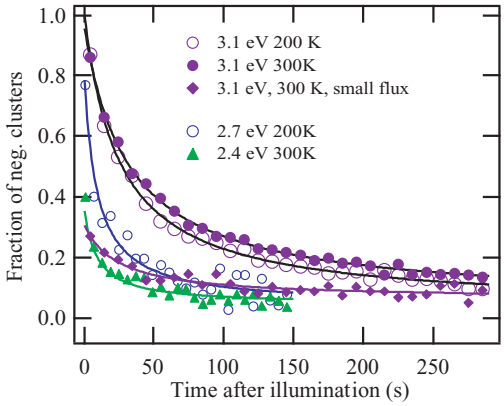

Figure 5.4. Fraction of negative clusters as a function of time after switching the illumination off. The measurement temperature is indicated. The fits are based on equation 2.9. The fluxes on the samples were $2\times10^{16}\mathrm{cm}^{-2}\mathrm{s}^{-1}$ at 3.1 eV, $4\times10^{16}\mathrm{cm}^{-2}\mathrm{s}^{-1}$ at 2.7 eV and $2\times10^{16}\mathrm{cm}^{-2}\mathrm{s}^{-1}$ at 2.4 eV. Further, a smaller flux of $4\times10^{14}\mathrm{cm}^{-2}\mathrm{s}^{-1}$ was used, yielding similar results for g at 3.1 eV.

5.3. Time slots of 0.5 s were used. At time -10 s the illumination is switched on. The onset of the illumination effect is very rapid, as at -9.5 s the average lifetime is close to the eventual saturation value. When the illumination is switched off, the average positron lifetime starts to decay. The complete decay of the photoexcitation effect takes several minutes. In the case of the 3.1 eV illumination, the cycle was 300 s long after switching off the light. Even after 300 s the average positron lifetime is 10 ps above the value in the dark. The onset of the illumination effect can be analysed based on equation 2.6 and the decay rate g can be estimated. However, the analytical solution of the equation is complicated, and the rapid onset of the illumination effect means that there are only a few experimental data points. Thus estimating g based on the decay of the photoexcitation is a simpler procedure.

When studying the decay of the photoexcitation effect, the fraction of negative clusters can be estimated with equation 3.30. The decay of the fraction of the negative vacancy clusters is shown in figure 5.4. The fits are based on equation 2.9, and the fitted values of g are shown in table 5.2. The fits match the experimental data very well, especially considering the small number of fitting parameters. Interestingly the decay is much slower at 3.1 eV than at 2.7 and 2.4 eV.

The photoexcitation model presented in section 2.3 assumes that free holes are generated from the valence band at the same rate as negative vacancies. In order to verify this, the decay of photoconductivity was measured. The measurements were conducted using the van der Pauw method [64] at photon energies 3.1 eV and 2.7 eV. The photoconductivity data is shown in figure 5.5. The

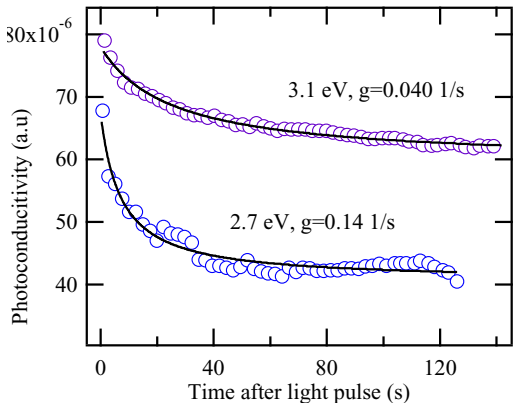

Figure 5.5. The decay of photoconductivity after a light pulse. The measurements were conducted at room temperature.

fits are based on the same model as in the positron measurements, i.e., using equation 2.9. During the first 100 ms the decay of the photocurrent is very rapid (not shown) but after that the decay behaviour is very similar to that obtained using positron measurements. This suggests that both the positron and the photoconductivity effects originate from the same processes.

The intensity of the illumination flux does not affect the decay rate g in the time-dependent measurements. This is interesting, since based on equation 2.7 the decay rate should decrease as the fraction of negative clusters decreases in the steady state. The flux-dependent steady-state measurements also suggest that g is constant. A possible explanation for this could be that the hole capture cross section is inversely proportional to the negative vacancy cluster concentration. Another possibility is that the hole concentration does not increase proportionally to the negative cluster concentration. However, the exact origin of the effect cannot be analysed based on these measurements alone. It should be noted that, e.g., a stretched exponential [89, 90] of the form $[V^-] = [V_0^-]\exp(-(gt)^\alpha)$, where $0 < \alpha < 1$, can be used to fit the experimental data. However, the stretched exponential assumes one fitting parameter more than our model, and the fit is not better than the one given by the original model.

The optical absorption cross section σ_{abs} can be estimated since the values of g/σ_{abs} and g are known. The values at different measurement points are listed in table 5.2. The vacancy concentration can also be estimated with the equation $\alpha = \sigma_{abs}[V]$. The absorption coefficient is α is 0.7 cm^{-1} at 3.1 eV for the unannealed diamond, yielding a vacancy cluster concentration of $[V] = 4 \times 10^{15}\text{cm}^{-3}$.

Table 5.2. Fit parameters and resulting optical cross sections listed for different wavelengths and temperatures.

Wavelenght	g/σ (10^{15}cm^{-2}s^{-1})	g (1/s)	σ_{abs} (10^{-18}cm^2)
2.4 eV, 300 K	2.87	0.148	50
2.7 eV, 200 K	2.19	0.125	100
3.1 eV, 300 K	0.188	0.0317	160
3.1 eV, 200 K	0.241	0.0354	150

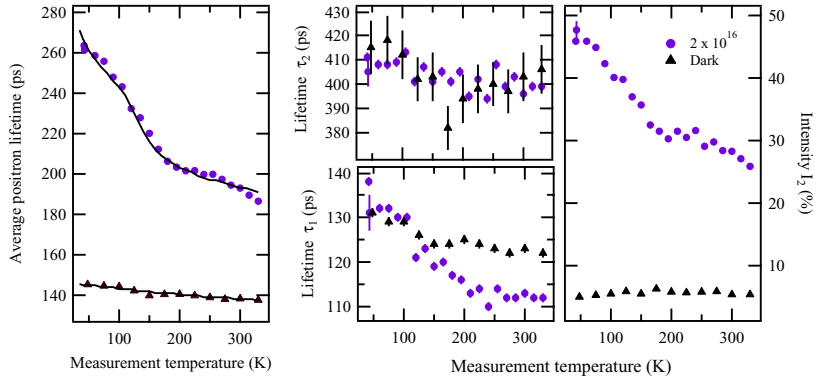

Figure 5.6. Average positron lifetime, lifetime components and intensity of the longest component, under 3.1 eV photoexcitation and in the dark.

5.3 Temperature dependence and trapping to vacancy clusters

The positron lifetime in brown diamond was measured as a function of temperature in order to obtain more information on the trapping processes of positrons to the defects. The measurements were conducted under 3.1 eV illumination and in the dark. The average lifetime, the lifetime components, and the intensity of the second component are shown in figure 5.6. The increase of the average lifetime due to the illumination is colossal, especially at low temperatures. When the measurement temperature increases, the average lifetime decreases, but even at 300 K it is about 50 ps above the value in the dark. The illumination flux was high, 2×10^{16}cm^{-2}s^{-1}, resulting in the saturation of the positron lifetime effect. When the sample is illuminated with a smaller flux (not shown), the qualitative shape of the average lifetime curve does not change, but the values shift downwards. In the dark the effect of temperature on the lifetime was considerably smaller.

Based on the experimental data it is clear that the intensity of the longest lifetime component governs the behaviour of the average lifetime, since the

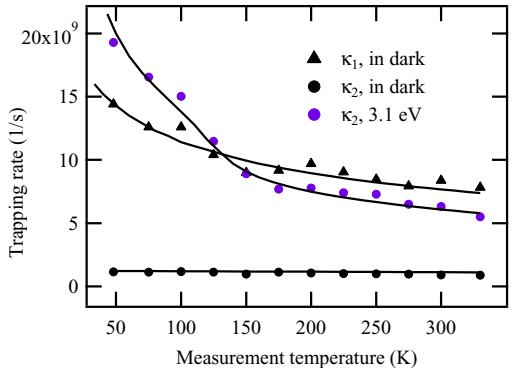

Figure 5.7. Trapping rates as a function of temperature.

illumination does not affect the values of the lifetime components. It could be argued that the decrease of average lifetime at higher temperatures could due to (i) decrease of the trapping coefficient or (ii) the increase of the decay rate g of the photoexcitation effect. However, the decay rate of the photoexcitation effect varies very little as a function of temperature. Interestingly, the rate is slightly higher at low temperature. The decay rates g vary from 0.06 s^{-1} at 45 K to 0.03 s^{-1} at 300 K. This implies that the fraction of negative clusters given by equation 2.6 is in the region 0.98-0.99 through the whole temperature range when the photon flux is high $2 \times 10^{16} cm^{-2} s^{-1}$. Thereby the variation of decay rate g as a function of temperature has a negligible effect on the positron lifetime parameters. It can be concluded that the effect seen as a function of measurement temperature is due to the decrease of the trapping coefficient with increasing temperature.

The temperature dependence is similar to that observed in gallium arsenide (GaAs) under illumination [76]. There positrons are attracted to shallow Rydberg-like states of negative vacancies. Positron trapping can be analysed in detail by estimating the trapping rates using equations 3.18 and 3.19. The estimated trapping rates in the dark and under illumination are shown in figure 5.7. The trapping rate κ_1 under illumination is not shown because the trapping seems to approach saturation at low temperatures below 200 K. The value of κ_2 under illumination has hence been estimated using κ_1 in the dark. In the dark κ_2 is constant as a function of temperature, implying that the defect is in the neutral charge state and the trapping is transition limited. κ_1 shows a small temperature dependence, i.e., $\kappa_1 \approx T^{-0.3}$. This behaviour could originate from the fact that if neither the diffusion nor transition limited trapping dominates, and the total trapping rate is a superposition of these two, as given by equation 3.5.

The trapping rate κ_2 in figure 5.7 is fitted by assuming that the trapping rate

to vacancy clusters is a sum $\kappa_2 = \kappa_{V,Ry} + \kappa_V$, where $\kappa_{V,Ry}$ is the trapping rate to Rydberg-like states and κ_V the trapping rate to the ground state of a negative vacancy. The trapping coefficient to Rydberg states is given by equation 3.3. It can be concluded that based on the temperature dependence of the positron trapping rate to the vacancy clusters, the clusters are neutral in the dark. The presence of Rydberg-like precursor states is a clear indication that the clusters become negatively charged under illumination.

In summary, application of the optical transient positron lifetime technique has been demonstrated. The method has been applied to brown natural diamond. Using transient and steady-state optical measurements, the value of the optical absorption cross section of vacancy clusters in brown diamond has been obtained. The measurements as a function of temperature show that clusters become negatively charged under illumination.

6. Identifying V_{Al} related defects in single-crystal AlN

In this chapter AlN single crystals have been studied in order to identify the nature of the cation vacancies and their decoration. Negative Al vacancies are present in the PVT AlN crystals. By combining coincidence-Doppler broadening measurements with ab-initio theoretical calculations it is shown that in-grown Al vacancies are complexed with O impurities, while proton irradiation produces mainly isolated Al vacancies. Finally, the optical absorption has been used to study the UV wavelength absorption caused by the vacancies.

6.1 Identification of negative Al vacancy

Several AlN bulk crystals, grown using PVT method, have been studied. The samples contain large concentrations of impurities, mostly O and C, which can potentially behave as shallow traps for positrons [91]. The positron lifetime results are shown in figure 6.1. The second lifetime component is shown when the decomposition of the spectrum is possible. At room temperature, the average lifetimes are in the region of 158-165 ps. The average lifetime for each sample is constant as a function of temperature below 300 K. Above 300 K the average lifetime starts increasing. The increase is due to detrapping of positrons from negative ions, as has been reported, e.g., in the case of GaN [92]. However, the increase of the average lifetime starts at rather high temperatures and still continues at 600 K, suggesting that the negative ions are at least doubly negative [93].

At high temperatures, above 500 K, a second lifetime component of 210 ± 5 ps can be fitted to the lifetime spectrum. The difference of the 210 ps lifetime component and that of the defect-free AlN lattice, estimated based on the τ_{ave} at low temperature is 55 ± 15 ps. The difference is close to 60, which is the theoretically calculated difference between the AlN lattice and the Al vacancy. In comparison, the lifetime difference between the AlN lattice and the N vacancy

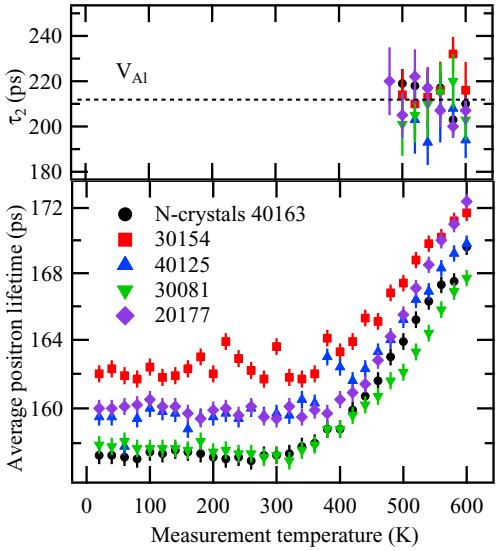

Figure 6.1. Average positron lifetime as a function of temperature in as grown AlN substrates.

is only 5 ps, suggesting that the 210 ps component corresponds to Al vacancies. Further, most of the calculations on AlN suggest that the N vacancy is in a positive charge state and thus is not able to trap positrons at all.

A better estimate of the positron lifetime in the AlN lattice can be obtained by selecting the second lifetime component as a constant 210 ps. At high temperatures the detrapping from the negative ions is rapid and the shorter component is given by $\tau_1 = (\lambda_B + \kappa_V)^{-1}$. At low temperatures, the trapping fraction η_V to the vacancy defects nearly vanishes and the value of τ_1 approaches that of the positron lifetime in the delocalized state τ_B. At 20 K, τ_1=155 ±1 ps and τ_{ave}=158, suggesting that the positron lifetime in the AlN lattice is between these two values, i.e., τ_B = 157 ps ± 1 ps.

6.2 Al vacancy-impurity complexes

Coincidence Doppler broadening has been used to identify in-grown and irradiation induced defects and their decoration in PVT grown AlN single crystals. The samples include an as-grown sample and a sample that has been irradiated with 9 MeV protons to a dose of 1×10^{16}cm^{-2}. Positron lifetime measurements were performed as a function of temperature in order to estimate the trapping fraction at Al vacancies. The trapping fractions were used to extract the vacancy specific Doppler spectrum. This was compared to ab-initio calculations in order to identify the in-grown and irradiation induced defect types. Further,

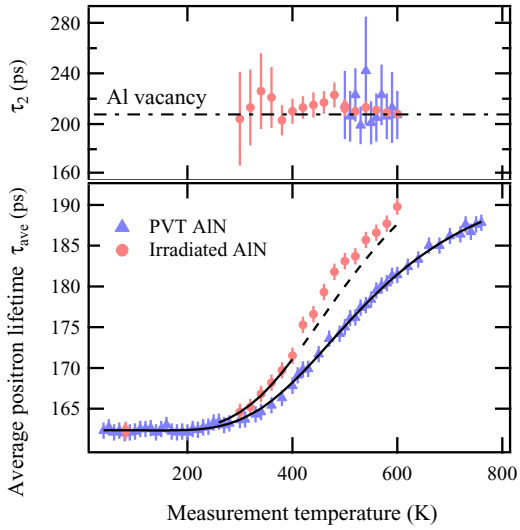

Figure 6.2. Average positron lifetime as a function of temperature in as grown and in irradiated AlN substrates.

transmission measurements in the visible and UV wavelengths were performed to identify the absorption peaks of different defect types.

The as-grown and irradiated samples were measured with positron lifetime spectroscopy in order to estimate the trapping fraction to vacancies and to estimate the increase in vacancy concentration due to the irradiation. The average positron lifetimes of the as-grown and irradiated samples are shown in figure 6.2. As previously explained, the increase of temperature increases the thermal escape of positrons from negative ions, increasing the annihilation signal from the vacancies. The average positron lifetime increases to 190 ps at 600 K compared to 181 ps in the as-grown case, indicating that vacancies have been generated.

The temperature dependent behaviour of the average lifetime has been analysed based on the kinetic trapping model for positrons. The Al vacancy and the negative ion concentrations can be obtained from the behaviour of the average lifetime as a function of temperature by taking into the account the thermal escape of positrons from the Rydberg states of the negative ions using equation 3.2. The annihilation fraction for vacancies is given by $\eta_V = \kappa_V/(\tau_B^{-1} + \kappa_V)$ and the trapping coefficient used for negative vacancies and ions $\mu_V = 3 \times 10^{15} \times (\frac{300K}{T})^{1/2}$. By combining these with equations 3.2 and 3.15-3.22 the average positron lifetime shown in figure 6.2 can be fitted.

The fit agrees with the experimental data very well for the as grown sample and for the irradiated sample up to the temperature of 400 K. It is possible that

clustering of vacancy defects takes place above 400 K in the irradiated sample, resulting in a more complex behaviour of the average lifetime. For the as-grown sample, the Al vacancy concentration has been estimated as $1 \times 10^{18}\text{cm}^{-3}$ and the negative ion concentration as $1 \times 10^{19}\text{cm}^{-3}$. The corresponding values for the irradiated sample are $4 \times 10^{18}\text{cm}^{-3}$ and $3 \times 10^{19}\text{cm}^{-3}$, respectively. The binding energy to the shallow traps is determined to be E_b=140 meV ± 5 meV in both cases, suggesting that the negative ions are at least doubly negative [93].

Coincidence Doppler broadening measurements were performed in order to identify the decoration of the Al vacancy. The samples were measured at elevated temperatures in order to extract the vacancy-specific Doppler spectrum. The as-grown sample was measured at 600 K in order to minimise the number of positrons annihilating bound to negative ions, whereas the irradiated sample had to be measured at 400 K in order to avoid the recovery of the irradiation-induced vacancies. Based on equation 3.22, the average lifetime can be written as $\tau_{ave} = (1-\eta_V)\tau_B + \eta_V \tau_V$. The trapping fraction can be solved as $\eta_V = (\tau_{ave} - \tau_B)/(\tau_V - \tau_B)$. The fraction of positrons annihilating in the Al vacancies is estimated to be 43 % for the as grown sample and 27 % for the irradiated sample at the measurement temperature. The annihilation fraction is used to extract the vacancy-specific Doppler spectrum. The experimental Doppler spectrum is given by equation 3.25, i.e. it as a weighted sum of contributions from a defect-free lattice and a vacancy or vacancies. By calculating the spectrum relative to the AlN lattice, the vacancy-specific spectrum can be written as $R_V = (R + \eta_V - 1)/\eta_V$, where $R_V = \rho_{meas}/\rho_B$.

Figure 6.3 shows the experimental ratios (relative to the AlN lattice) for the as-grown and the irradiated samples in the upper panel. The theoretical intensity ratios of different vacancy configurations are shown in the lower panel. The experimental spectra have been normalised relative to the AlN crystal with the lowest measured average lifetime ($\tau_{ave} \approx \tau_B$). Experimental data of the as-grown samples matches the calculated Al-vacancy-O-atom-complex ($V_{Al} - O_N$) very well, especially at around 1.5 a.u. Adding more O atoms increases the height of the shoulder at 1.5 a.u. further (not shown), suggesting that there is only a single O atom neighbouring the Al vacancy. The other of the calculated configurations, i.e., Al vacancy-N vacancy pair ($V_{Al} - V_N$), Al-vacancy-hydrogen pair ($V_{Al} - H$) and the isolated Al vacancy (V_{Al}) result in a lower shoulder at 1.5 a.u. This suggests that in the as-grown samples the Al vacancy always neighbours an O atom. The increased shoulder caused by O atoms seem to be typical of III-nitrides in general: a similar shoulder is detected in the case of

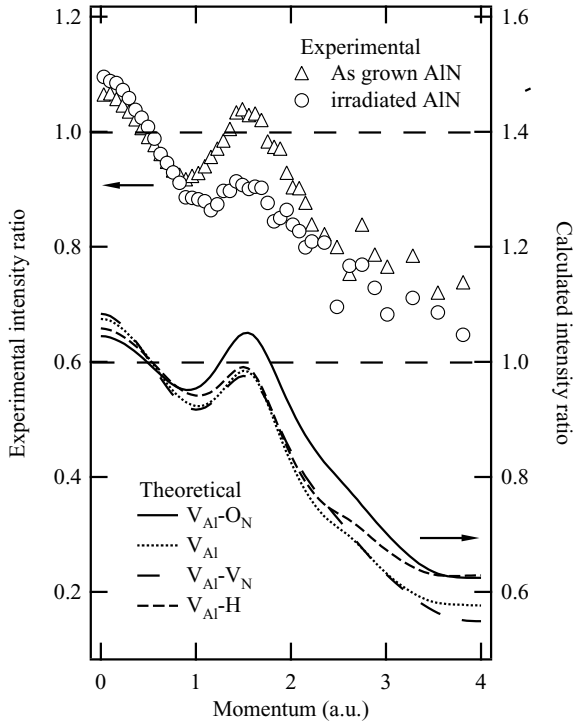

Figure 6.3. Experimental (upper panel) and theoretical (lower panel) coincidence Doppler ratio curves corresponding to different vacancy configurations.

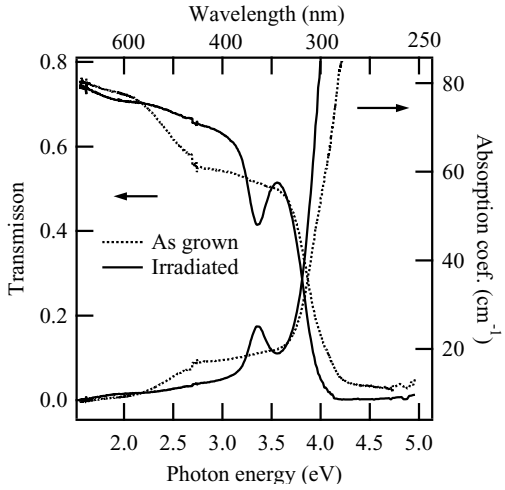

Figure 6.4. Transmission and uncorrected absorption spectra for as-grown and irradiated AlN at wavelenghts 800-260 nm.

GaN [94] and InN [95]. In the case of the irradiation induced vacancies, the experimental curve clearly does not correspond to $V_{Al} - O_N$ but it is not possible to distinguish which one of the curves $V_{Al} - V_N$, $V_{Al} - H$, and V_{Al} result in the best correspondence to the experimental data. However, it can be expected that isolated Al vacancies are generated during the irradiation. Also N vacancies are generated, but most probably those are not generated next to the Al vacancies with the high energy (9.5 MeV) protons. Individual N vacancies are not detected with positrons due to their positive charge state [8]. Hence, the vacancies detected in the irradiated AlN sample are identified as isolated Al vacancies.

The coincidence Doppler measurements strongly suggests that the in-grown Al vacancies are decorated by O atoms. The O concentration given by gas discharge mass spectroscopy (GDMS) is less than 10^{18} cm^{-3} [91], which is comparable to the Al vacancy concentration of 10^{18} cm^{-3} estimated by positron lifetime spectroscopy. Thus, most, if not all, O atoms are decorated by Al vacancies. Therefore the key in decreasing the vacancy content in AlN is to limit the O concentration.

The optical transparency of the AlN is critical when it is employed as substrates in optoelectronic devices. Absorption measurements were performed at wavelengths 800-260 nm in order to study the influence of vacancies on the optical transparency. The transmission coefficient and the uncorrected optical absorption (reflectance not taken into account) are plotted in figure 6.4. Features of the irradiated sample's spectrum include a decrease of the absorption at 2.5-3.1 eV, an absorption peak at 3.4 eV, and possibly an increase of the ab-

sorption at energies higher than 4.0 eV. The decrease of absorption at 2.5-3.1 eV is attributed to the movement of the Fermi level, possibly changing the occupation of some unknown defect levels, possibly that of the $V_{Al} - O_N$. However, the exact identification of the defect level is not possible based on these measurements alone. The absorption peak at 3.4 eV is clearly due to a transition between two bound states. The Al and N vacancies are predicted to have energy levels energy levels in the range of 2.0-2.5 eV [58, 59] and at 5.9 eV [53] above the valence band edge, respectively. Therefore the absorption peak at 3.4 could be a charge transfer process between the Al and N vacancies. Both V_{Al} and V_N are certainly generated during the irradiation.

In conclusion, the as-grown AlN contains Al vacancies with $V_{Al} - O_N$ being the dominant form. The in-grown Al vacancy concentration is 3×10^{18} cm^{-3}. The Al vacancies generated by proton irradiation are isolated. The absorption measurements suggest that Al vacancies cause optical absorption in the UV region.

7. Summary

In this thesis, vacancy-type defects and their influence on the optical properties of diamond and AlN were studied. In Publ. I the origin of brown colour in high-purity natural diamond was analysed. The brown colour is caused by an absorption ramp starting at 2.0 eV. The absorption is not caused by impurities, since type IIa diamond contains only a small concentration of them. The brown colour is gradually lost during HPHT treatment, suggesting that the defects causing the colour dissociate. Positron measurements show that the untreated brown diamond contains vacancy clusters with a 400 ps positron lifetime component, corresponding to 40-60 missing atoms. Further, a lifetime component with open volume roughly that of a monovacancy was detected. The component is probably related to dislocations. Positron lifetime measurements show that the vacancy clusters are optically active. The vacancy clusters charge negatively when they are illuminated with visible light. During HPHT treatment the vacancy clusters dissociate in correlation with the reduction of brown colour. It can be concluded that the brown colour in natural high-purity diamond is caused by vacancy clusters, giving a 400 ps positron lifetime component.

A new method, optical transient positron spectroscopy, was developed in order to study the optical properties of vacancies. The method was applied to natural diamond in order to obtain information about the microscopic nature of the charge-transfer processes behind the brown colouration. The work has been reported in Publs. II and III. Natural diamond shows a colossal increase of average positron lifetime due to the 400 ps component, enabling us to concentrate on the optical effect. The transient optical method provides information on the time scales of the charge transfer processes related to the vacancy clusters. By combining flux-dependent measurements with the decay rates of the photoexcitation effects, the optical absorption cross section of the clusters causing the brown colouration can be determined and the vacancy cluster concentration estimated self-consistently. The optical absorption cross sec-

tion is σ_{abs}=150×10^{-18}cm^2 at 3.1 eV and the vacancy cluster concentration of the measured sample is 4×10^{16}cm^{-3}. It is worth noting that this is the first time that the defect concentration has been estimated using positron lifetime spectroscopy self-consistently without assumed knowledge of the trapping coefficient. The diamond samples also exhibit photoconductivity. The transient behaviour of photoconductivity is very similar to that seen with positron experiments. Even though the exact origin of photoconductivity can not be pinpointed, the similar time constant suggests that vacancy clusters give rise to photoconductivity.

In Publs. IV and V, Al vacancies in PVT grown AlN are studied. Positron lifetime measurements show that Al vacancies are present in the samples, along with a high concentration of negative ions (possibly related to the C or O atoms). The temperature-dependent behaviour of the positron lifetime suggests thats Al vacancies are in a negative charge state. The chemical surrounding of the Al vacancies was studied using coincidence Doppler broadening spectroscopy. PVT-grown AlN was measured as-grown and after proton irradiation with a dose of 1×10^{16}cm^{-2}. The experimental coincidence Doppler ratio curves were compared to theoretical ones obtained from ab-initio calculations. The theoretical curves were calculated for different impurity atoms and defect configurations. The measurements clearly show that Al vacancies in as-grown samples are decorated by O atoms, suggesting that most, if not all, O atoms have neighbouring Al vacancies. It is likely that O atoms stabilise mobile Al vacancies during PVT growth. Hence, reducing the O content is the key to improving the quality of AlN crystals. Coincidence Doppler measurements indicate that proton irradiation generates isolated Al vacancies. Absorption measurements show that after the irradiation there is an additional absorption peak at 3.4 eV. The absorption peak can be attributed to a charge-transfer transition between Al and N vacancies. The results show that Al vacancies can cause absorption at UV wavelengths.

Bibliography

[1] M. Levinstein, S. Rumyantsev, and M. Shur, *Handbook Series on Semiconductor Parameters* (World Scientific, London, 1996).

[2] H.O. Pierson, *Handbook of Carbon, Graphite, Diamond and Fullerenes - Properties, Processing and Applications* (William Andrew Publishing, Norwich, US, 1993).

[3] J.H. Edgar, *Properties of Group III Nitrides* (Institution of Engineering and Technology, Stevenage, UK, 1994).

[4] M. Nesladek, Semicond. Sci. Technol. **20**, R19 (2005).

[5] Y. Taniyasu, M. Kasu, and T. Makimoto, Nature **441**, 325 (2006).

[6] J. Wilks and E. Wilks, *Properties and Applications of Diamond* (Butterworth-Heinemann, Oxford, U.K., 1991).

[7] R. Krause-Rehberg and H. S. Leipner, *Positron Annihilation in Semiconductors* (Springer, New York, 1999).

[8] K. Saarinen, P. Hautojärvi, and C. Corbel, in *Identification of Defects in Semiconductors*, edited by M. Stavola (Academic Press, San Diego, 1998), Vol. 51A, p. 209.

[9] P. Hautojärvi and C. Corbel, in *International School of Physics Enrico Fermi, Course CXXV*, edited by A. Dupasquier (IOS Press, Amsterdam, 1993).

[10] M. J. Puska and R. M. Nieminen, Rev. Mod. Phys. **66**, 841 (1994).

[11] I. Makkonen, M. Hakala, and M. J. Puska, Phys. Rev. B **73**, 035103 (2006).

[12] L. Wei, P. K. Kuo, R. L. Thomas, T. R. Anthony, and W. F. Banholzer, Phys. Rev. Lett. 3764 (1993).

[13] D.R. Kania, M.I. Landstrass, and M.A. Plano, Diamond Relat. Mater. 1012 (1993).

[14] J. Isberg, J. Hammersberg, E. Johansson, T. Wikström, D.J. Twitchen, A. J Whitehead, S. E. Coe, and G.A. Scarsbrook, Science (New York, N.Y.) **297**, 1670 (2002).

[15] G.A.J Amaratunga, Science (New York, N.Y.) **297**, 1657 (2002).

[16] W. Kaiser and W. L. Bond, Phys. Rev. **115**, 857 (1959).

[17] R.G. Farrer, Solid State Commun. **7**, 685 (1969).

[18] G. Davies, *Properties and growth of Diamond* (Institute of Electrical Engineers, Stevenage, UK, 1994).

[19] K. Iakoubovskii and A. Stesmans, J. Phys.: Condens. Matter **14**, R467 (2002).

[20] A.T. Collins, Diamond Relat. Mater. **8**, 1455 (1999).

[21] J.A. van Wyk, J. Phys. C: Solid State Phys. **15**, L981 (1982).

[22] A.T. Collins, Philos. Trans. R. Soc. London, Ser. A **342**, 233 (1993).

[23] M. V. Gurudev Dutt, L. Childress, L. Jiang, E. Togan, J. Maze, F. Jelezko, A. S. Zibrov, P. R. Hemmer, and M. D. Lukin, Science **316**, 1312 (2007).

[24] J. R. Maze, P. L. Stanwix, J. S. Hodges, S. Hong, J. M. Taylor, P. Cappellaro, L. Jiang, M. V. Gurudev Dutt, E. Togan, A. S. Zibrov, A. Yacoby, R. L. Walsworth, and M. D. Lukin, Nature **455**, 644 (2008).

[25] J. R. Rabeau, P. Reichart, G. Tamanyan, D. N. Jamieson, S. Prawer, F. Jelezko, T. Gaebel, I. Popa, M. Domhan, and J. Wrachtrup, Appl. Phys. Lett. **88**, 023113 (2006).

[26] E. Fritsch, *The nature of Diamonds ed G E Harlow* (Cambridge University Press, UK, 1998), pp. 23–47.

[27] M. L. Johnson, Koivula J. I., McClure S. F., and DeGhionno D., Gems Gemol. **35**, 144 (1999).

[28] T. M. Moses, J. E. Shigley, S. F. McClur, J. I. Koivula, and M. van Daele, Gems Gemol. **35**, 14 (1999).

[29] A. Collins, H. Kanda, and H. Kitawak, Diamond Relat. Mater. **9**, 113 (2000).

[30] C Fall, A Blumenau, R Jones, P Briddon, T Frauenheim, a. Gutiérrez-Sosa, U Bangert, a. E. Mora, J Steeds, and J Butler, Phys. Rev. B **65**, 1 (2002).

[31] B. Willems, P. M. Martineau, D. Fisher, J. van Royen, and G. van Tendeloo, Physica Status Solidi (a) **203**, 3076 (2006).

[32] V Avalos and S Dannefaer, Physica B: Condensed Matter **340-342**, 76 (2003).

[33] R. Barnes, U. Bangert, and P. Martineau, Physica Status Solidi (a) **203**, 3081 (2006).

[34] R Barnes, U Bangert, and a. Scott, Physica Status Solidi (a) **204**, 3065 (2007).

[35] U. Bangert, R. Barnes, M. H. Gass, A. L. Bleloch, and I. S. Godfrey, J. Phys.: Condens. Matter **21**, (2009).

[36] I. S. Godfrey and U. Bangert, J. Phys.: Conf. Series **281**, 012024 (2011).

[37] L. S. Hounsome, R. Jones, P.M. Martineau, M.J. Shaw, P.R. Briddon, S. Öberg, A.T. Blumenau, and N. Fujita, Physica Status Solidi (a) **202**, 2182 (2005).

[38] L. S. Hounsome, R. Jones, P. Martineau, D. Fisher, M. Shaw, P. Briddon, and S. Öberg, Physical Review B **73**, 1 (2006).

[39] R Jones, Diamond Relat. Mater. **18**, 820 (2009).

[40] N Fujita, R Jones, S Öberg, and P. R. Briddon, Diamond Relat. Mater. **18**, 843 (2009).

[41] I. Laszlo, M. Kertesz, B. Slepetz, and Y. Gogotsi, Diamond Relat. Mater. **19**, 1153 (2010).

[42] P. Lu, R. Collazo, R. F. Dalmau, G. Durkaya, N. Dietz, and Z. Sitar, Appl. Phys. Lett. 131922 (2008).

[43] G. A. Slack, L. J. Schowalter, D. Morelli, and J. A. Freitas, J. Cryst. Growth 287 (2002).

[44] A. S. Segal, S. Y. Karpov, Y. N. Makarov, E. N. Mokhov, A. D. Roenkov, M. G. Ramm, and Y. A. Vodakov, J. Cryst. Growth 68 (2000).

[45] R. Schlesser, R. Dalmau, and Z. Sitar, J. Cryst. Growth 416 (2002).

[46] B. M. Epelbaum, C. Seitz, A. Magerl, M. Bickermann, and A. Winnacker, J. Cryst. Growth 577 (2004).

[47] J. C. Rojo, G.A. Slack, K.Morgan, B. Raghothamachar, M.Dudley, and L. J. Schowalter, J. Cryst. Growth 317 (2001).

[48] S. Krukowski, A. Witek, J. Adamczyk, M. Bockowski J. Jun, I. Grzegory, B. Lucznik, G. Nowak, M. Wróblewski, A. Presz, S. Gierlotka, S. Stelmach, B. Palosz, S. Porowski, and P. Zinn, J. Phys. Chem. Solids **59**, 289 (1998).

[49] B. D. Schultz, A. Argoitia, C. C. Hayman, J. C. Angus, J. S. Dyck, K. Kash, and Y. Nan, Proceedings of the Third Symposium on IIIV Nitride Materials and Processes Electrochem Soc 1999, Pennington, USA 108 (1999).

[50] V. Avrutin, D. J. Silversmith, Y. Mori, F. Kawamura, Y. Kitaoka, and H. Morkoc, Proc. IEEE **98**, 1302 (2010).

[51] Y. Makarov, O. Avdeev, I. Barash, D. Bazarevskiy, T. Chemekova, E. Mokhov, S. Nagalyuk, A. Roenkov, A. Segal, and Y. Vodakov, J. Cryst. Growth **310**, 881 (2008).

[52] Z. Gu, L. Du, J. H. Edgar, N. Nepal, J.Y. Lin, H.X. Jiang, and R. Witt, J. Cryst. Growth **297**, 105 (2006).

[53] N. Nepal, K. B. Nam, M. L. Nakarmi, J. Y. Lin, H. X. Jiang, J. M. Zavada, and R. G. Wilson, Appl. Phys. Lett **84**, 1090 (2004).

[54] B. Bastek, F. Bertram, J. Christen, T. Hempel, A. Dadgar, and A. Krost, Appl. Phys. Lett. **95**, 032106 (2009).

[55] T. Schulz, M. Albrecht, K. Irmscher, C. Hartmann, J. Wollweber, and R. Fornari, Phys. Status Solidi B **248**, 1513 (2011).

[56] T. Mattila and R.M. Nieminen, Phys. Rev. B. **55**, 9571 (1997).

[57] I. Gorczyca, A. Svane, and N. E. Christensen, Phys. Rev. B **60**, 8147 (1999).

[58] C. Stampfl and C. Van de Walle, Phys. Rev. B **65**, 1 (2002).

[59] Y. Zhang, W. Liu, and H. Niu, Phys. Rev. B **77**, 1 (2008).

[60] K. Laaksonen, M. G. Ganchenkova, and R. M. Nieminen, J. Phys.: Condens. Matter **21**, 15803 (2009).

[61] T. Koyama, M. Sugawara, T. Hoshi, A. Uedono, J. F. Kaeding, R. Sharma, S. Nakamura, and S. F. Chichibu, Appl. Phys. Lett. **90**, 241914 (2007).

[62] A. Uedono, S. Ishibashi, S. Keller, C. Moe, P. Cantu, T. M. Katona, D. S. Kamber, Y. Wu, E. Letts, S. A. Newman, S. Nakamura, J. S. Speck, U. K. Mishra, S. P. DenBaars, T. Onuma, and S. F. Chichibu, J. Appl. Phys. **105**, 054501 (2009).

[63] K. Moazzami, T. E. Murphy, J. D. Phillips, M. C.-K. Cheung, and A. N. Cartwright, Semicond. Sci. Technol. **21**, 717 (2006).

[64] D. K. Schroder, *Semiconductor material and device characterization* (John Wiley & Sons, Inc., New York, 1998), p. 267.

[65] R. H. Bube, *Photoelectric properties of Semiconductors* (Cambridge University Press, UK, 1992).

[66] J. I. Pankove, *Optical Processes in Semiconductors* (Prentice-Hall, New Jersey, USA, 1971).

[67] M. Lax, Phys. Rev. **119**, 1502 (1960).

[68] J. I. Pankove, L. Tomasetta, and B. F. Williams, Phys. Rev. Lett. **27**, 29 (1971).

[69] P. J. Dean, Prog. Crystal Growth Charact **5**, 89 (1982).

[70] K. R. Rebane, J. Lumin. **86**, 167 (2000).

[71] D. V. Lang, J. Appl. Phys. **45**, 3023 (1974).

[72] C. H. Hurtes, M. Boulou, A. Mitonneau, and D. Bois, Appl. Phys. Lett. **32**, 821 (1978).

[73] J. Mäkinen, P. Hautojärvi, and C. Corbel, J. Phys.: Condens. Matter **4**, 5137 (1992).

[74] A. Kawasuso, H. Masayuki, S. Masashi, Y. Sadae, and S. Koji, Jpn. J. Appl. Phys. **34**, 2197 (1995).

[75] M. J. Puska, C. Corbel, and R. M. Nieminen, Phys. Rev. B **41**, 9980 (1990).

[76] C. Le Berre, C. Corbel, K. Saarinen, S. Kuisma, P. Hautojärvi, and R. Fornari, Phys. Rev. B **52**, 8112 (1995).

[77] P. Asoka-Kumar, M. Alatalo, V. J. Ghosh, A. C. Kruseman, B. Nielsen, and K. G. Lynn, Phys. Rev. Lett. **77**, 2097 (1996).

[78] K. Saarinen, S. Kuisma, P Hautojärvi, C. Corbel, and C. LeBerre, Phys. Rev. Lett. **70**, 2794 (1993).

[79] S. Kuisma, K. Saarinen, P. Hautojärvi, C. Corbel, and C. LeBerre, Phys. Rev. B **53**, 9814 (1996).

[80] S. Kuisma, K. Saarinen, P. Hautojärvi, and C. Corbel, Phys. Rev. B **55**, 9609 (1997).

[81] S.-L. Sihto, J. Slotte, J. Lento, K. Saarinen, E. V. Monakhov, A. Yu. Kuznetsov, and B. G. Svensson, Phys. Rev. B **68**, 115307 (2003).

[82] F. Tuomisto, K. Saarinen, D. C. Look, and G. C. Farlow, Phys. Rev. B **72**, 085206 (2005).

[83] A. Uedono, S. Fujii, N. Morishita, H. Itoh, S. Tanigawa, and S. Shikata, J. Phys.: Condens. Matter **11**, 4109 (1999).

[84] A. Pu, T. Bretagnon, D. Kerr, and S. Dannefaer, Diamond Relat. Mater. **9**, 1450 (2000).

[85] A Uedono, K Mori, N Morishita, H Itoh, S Tanigawa, S Fujii, and S Shikata, J. Phys.: Condens. Matter **11**, 4925 (1999).

[86] T. Torsti, T. Eirola, J. Enkovaara, T. Hakala, P. Havu, V. Havu, T. Höynälänmaa, J. Ignatius, M. Lyly, I. Makkonen, T. T. Rantala, J. Ruokolainen, K. Ruotsalainen, E. Räsänen, H. Saarikoski, and M. J. Puska, Phys. Stat. Sol.(b) **243**, 1016 (2006).

[87] A. Blumenau, M Heggie, C Fall, R Jones, and T Frauenheim, Phys. Rev. B **65**, 1 (2002).

[88] L. S. Hounsome, private communication, 2005.

[89] D. L. Huber, Phys. Rev. B **31**, 6070 (1985).

[90] J. Klafter and M. F. Shlesinger, Prc. Natl. Acad. Sci USA **83**, 848 (1986).

[91] T. Yu. Chemekova, private communication, 2010.

[92] K. Saarinen, T. Laine, S. Kuisma, J. Nissilä, P. Hautojärvi, L. Dobrzynski, J. M. Baranowski, K. Pakula, R. Stepniewski, M. Wojdak, A. Wysmolek, T. Suski, M. Leszczynski, I. Grzegory, and S. Porowski, Phys. Rev. Lett. **79**, 3030 (1997).

[93] F. Tuomisto, V. Ranki, D. C. Look, and G. C. Farlow, Phys. Rev. B **76**, 165207 (2007).

[94] S. Hautakangas, I. Makkonen, V. Ranki, M. J. Puska, K. Saarinen, X. Xu, and D. C. Look, Phys. Rev. B **73**, 193301 (2006).

[95] C. Rauch, I. Makkonen, and Tuomisto F., Phys. Rev. B **84**, 125201 (2011).

Aalto-DD 28/2012

ISBN 978-952-60-4545-0
ISBN 978-952-60-4546-7 (pdf)
ISSN-L 1799-4934
ISSN 1799-4934
ISSN 1799-4942 (pdf)

Aalto University
Name of the School
Department of Applied Physics
www.aalto.fi

BUSINESS +
ECONOMY

ART +
DESIGN +
ARCHITECTURE

SCIENCE +
TECHNOLOGY

CROSSOVER

**DOCTORAL
DISSERTATIONS**